

Contributions of Intrinsic Membrane Dynamics to Fast Network Oscillations With Irregular Neuronal Discharges

Caroline Geisler, Nicolas Brunel and Xiao-Jing Wang

JN 94:4344-4361, 2005. First published Aug 10, 2005; doi:10.1152/jn.00510.2004

You might find this additional information useful...

This article cites 69 articles, 44 of which you can access free at:

<http://jn.physiology.org/cgi/content/full/94/6/4344#BIBL>

Updated information and services including high-resolution figures, can be found at:

<http://jn.physiology.org/cgi/content/full/94/6/4344>

Additional material and information about *Journal of Neurophysiology* can be found at:

<http://www.the-aps.org/publications/jn>

This information is current as of November 22, 2005 .

Contributions of Intrinsic Membrane Dynamics to Fast Network Oscillations With Irregular Neuronal Discharges

Caroline Geisler,^{1,2} Nicolas Brunel,³ and Xiao-Jing Wang¹

¹Physics Department and Volen Center for Complex Systems, Brandeis University, Waltham, Massachusetts; ²Center for Molecular and Behavioral Neuroscience, Rutgers University, Newark, New Jersey; and ³Laboratory of Neurophysics and Physiology, Unité Mixte de Recherche 8119, Centre National de la Recherche Scientifique, Université Paris René Descartes, Paris, France

Submitted 16 May 2005; accepted in final form 3 August 2005

Geisler, Caroline, Nicolas Brunel, and Xiao-Jing Wang. Contributions of intrinsic membrane dynamics to fast network oscillations with irregular neuronal discharges. *J Neurophysiol* 94: 4344–4361, 2005. First published August 10, 2005; doi:10.1152/jn.00510.2004. During fast oscillations in the local field potential (40–100 Hz gamma, 100–200 Hz sharp-wave ripples) single cortical neurons typically fire irregularly at rates that are much lower than the oscillation frequency. Recent computational studies have provided a mathematical description of such fast oscillations, using the leaky integrate-and-fire (LIF) neuron model. Here, we extend this theoretical framework to populations of more realistic Hodgkin–Huxley-type conductance-based neurons. In a noisy network of GABAergic neurons that are connected randomly and sparsely by chemical synapses, coherent oscillations emerge with a frequency that depends sensitively on the single cell's membrane dynamics. The population frequency can be predicted analytically from the synaptic time constants and the preferred phase of discharge during the oscillatory cycle of a single cell subjected to noisy sinusoidal input. The latter depends significantly on the single cell's membrane properties and can be understood in the context of the simplified exponential integrate-and-fire (EIF) neuron. We find that 200-Hz oscillations can be generated, provided the effective input conductance of single cells is large, so that the single neuron's phase shift is sufficiently small. In a two-population network of excitatory pyramidal cells and inhibitory neurons, recurrent excitation can either decrease or increase the population rhythmic frequency, depending on whether in a neuron the excitatory synaptic current follows or precedes the inhibitory synaptic current in an oscillatory cycle. Detailed single-cell properties have a substantial impact on population oscillations, even though rhythmicity does not originate from pacemaker neurons and is an emergent network phenomenon.

INTRODUCTION

Spike trains of cortical neurons are usually very irregular and close to a Poisson process, even when the local field potential recordings exhibit coherent fast oscillations such as gamma oscillations (40–80 Hz) (Destexhe et al. 1999; Fries et al. 2001b; Pesaran et al. 2002) and sharp-wave ripples (100–200 Hz) (Buzsáki et al. 1992; Csicsvari et al. 1998, 1999a). In such oscillatory episodes, single-cell discharge rates are typically much lower than the oscillation frequency of the field potential.

Theoretical studies have demonstrated that such population rhythms appear in randomly connected networks of leaky integrate-and-fire (LIF) neurons, when the synaptic inhibitory feedback is strong and noise is sufficiently large (Brunel 2000; Brunel and Hakim 1999; Brunel and Wang 2003). Brunel and

Wang (2003) showed how the population rhythmic frequency of networks of inhibitory LIF neurons depends on the time constants of the recurrent synaptic currents. With physiologically reasonable time constants, the population frequency is >100 Hz and can be as high as 300 Hz, whereas single cells fire irregularly and at a much lower rate than the population frequency. It was then shown that in a two-population network of inhibitory and excitatory LIF neurons the population frequency depends both on the time constants of excitatory and inhibitory currents and on the relative strength of recurrent excitation and inhibition: the population frequency is decreased by the synaptic excitation. In the absence of recurrent excitation among pyramidal cells the population can oscillate at 200 Hz (as observed in the CA1 area of the rat hippocampus); if the recurrent excitation is sufficiently strong, the network frequency is decreased to 100 Hz.

In a network of LIF neurons, the frequency of coherent oscillations is essentially independent of the intrinsic single-cell properties because the spiking response of an LIF model to sinusoidal input in the presence of temporally correlated noise depends only weakly on the input oscillation frequency (Brunel et al. 2001). In particular, the phase shift of the instantaneous firing rate with respect to the periodic input is very small at any input frequency. Thus through the static current–frequency relationship, single-cell properties affect the degree of synchronization of the network but not the frequency of the network oscillation.

In this paper, we examine the generality of this conclusion and show that this no longer holds true for Hodgkin–Huxley-type conductance-based neurons. The LIF neuron integrates the synaptic inputs linearly until the membrane potential reaches a threshold and a spike is triggered instantaneously. This rigid threshold behavior of LIF neurons is only a rough approximation for the actual spike-generating mechanism. Real neurons do not have a unique spiking threshold (Azouz and Gray 2000). Even if one defines a spike threshold empirically, subthreshold membrane dynamics is highly nonlinear, unlike that in the LIF model. Furthermore, after crossing the threshold the depolarization takes about 0.2–1.5 ms to reach the voltage maximum (Buhl et al. 1994; Connors et al. 1982; Lacaille and Williams 1990; Nowak et al. 2003; Zhang and McBain 1995), in contrast to the LIF model that has no spike time to peak. The precise shape of the action potential is determined by the detailed kinetic properties of the spike-

Address for reprint requests and other correspondence: X.-J. Wang, Volen Center for Complex Systems, Brandeis University, Waltham, MA 02454 (E-mail: xjwang@brandeis.edu).

The costs of publication of this article were defrayed in part by the payment of page charges. The article must therefore be hereby marked "advertisement" in accordance with 18 U.S.C. Section 1734 solely to indicate this fact.

generating sodium and potassium currents (Lien et al. 2002; Martina and Jonas 1997; Martina et al. 1998). These biophysical properties of action potential generation give rise to strong frequency modulation of the single neuron responsiveness to a noisy sinusoidal input (see below and Fourcaud-Trocmé et al. 2003). Consequently, for the conductance-based models, single-neuron properties can be expected to play an important role in determining the frequency of network-generated fast coherent oscillations. The purpose of the present paper is to understand how single-neuron properties affect collective oscillations in the strong noise regime.

METHODS

Model neurons

INTERNEURON. Unless stated otherwise, the interneuron model used in the simulations is a conductance-based model that is slightly modified from Wang and Buzsáki (1996). It is a one-compartment model with a total surface area of 0.02 mm². The current balance equation obeys

$$C_m dV/dt = -I_L - I_{Na} - I_K - I_{syn} + I_{ext} \quad (1)$$

The capacitance of the membrane is $C_m = 0.2$ nF. The leak current $I_L = g_L(V - V_L)$ has the conductance $g_L = 0.02$ μ S and reversal potential $V_L = -67$ mV. I_{syn} is the synaptic input current and I_{ext} is an external applied current. The spike-generating ion currents $I_{Na} = g_{Na} m^3 h (V - V_{Na})$ and $I_K = g_K n^4 (V - V_K)$ are of the Hodgkin-Huxley type (Hodgkin and Huxley 1952). The voltage-dependent gating variables h and n are time dependent $dx/dt = \phi_x [\alpha_x(V)(1 - x) - \beta_x(V)x]$ with $x = \{h, n\}$, the voltage is measured in mV, and the rate functions $\alpha_x(V)$ and $\beta_x(V)$ are in ms⁻¹; $\alpha_h = 0.07 \exp[-0.05(V + 58)]$, $\beta_h = 1.0 / \{\exp[-0.1(V + 28)] + 1\}$ and $\alpha_n(V) = -0.01(V + 34) / \{\exp[-0.1(V + 34)] - 1\}$, $\beta_n(V) = 0.125 \exp[-0.0125(V + 44)]$. The activation variable m is assumed to be fast and is substituted by its steady state $m_\infty = \alpha_m / (\alpha_m + \beta_m)$; $\alpha_m(V) = -0.1(V + 35) / \{\exp[-0.1(V + 35)] - 1\}$ and $\beta_m(V) = 4 \exp[-(V + 60)/18]$. The maximal conductances are $g_{Na} = 14$ μ S and $g_K = 1.8$ μ S. The reversal potentials are $V_{Na} = 55$ mV and $V_K = -90$ mV. The temperature factors are $\phi_n = \phi_h = 5$.

INTERNEURON WITH A-TYPE CURRENT. In hippocampal interneurons a large variety of ion channels have been found including A-type potassium currents that are activated at subthreshold voltage (Erisir et al. 1999; Lien et al. 2002; Martina et al. 1998). This finding has motivated investigations of a neuronal model containing an A-type potassium current. It is a one-compartment model with a total surface area of 0.02 mm². The current balance equation obeys

$$C_m dV/dt = -I_L - I_{Na} - I_K - I_A - I_{syn} + I_{ext} \quad (2)$$

The capacitance of the membrane is $C_m = 0.2$ nF. The dynamics of the leak current I_L and the spike generating currents I_{Na} and I_K are the same as those given for the interneuron except $\alpha_h = 0.07 \exp[-0.05(V + 48)]$, $\beta_h = 1.0 / \{\exp[-0.1(V + 18)] + 1\}$ and $\alpha_n(V) = -0.01(V + 45.7) / \{\exp[-0.1(V + 45.7)] - 1\}$, $\beta_n(V) = 0.125 \exp[-0.0125(V + 55.7)]$, $\alpha_m(V) = -0.1(V + 29.7) / \{\exp[-0.1(V + 29.7)] - 1\}$ and $\beta_m(V) = 4 \exp[-(V + 54.7)/18]$. The maximal conductances are $g_L = 0.06$ μ S, $g_{Na} = 24$ μ S and $g_K = 4$ μ S. The reversal potentials are $V_L = -17$ mV, $V_{Na} = 55$ mV, and $V_K = -72$ mV. The temperature factors are $\phi_n = \phi_h = 3.8$. The kinetics of the A-type potassium current $I_A = g_A A_\infty^3 B (V - V_A)$ is the same as described in Connor et al. (1977), with $dB/dt = (B_\infty - B) / \tau_B$, where $A_\infty = 0.0761 \{\exp[(V + 94.22)/31.84] / \{1 + \exp[(V + 1.17)/28.93]\}\}^{(1/3)}$, $B_\infty = 1 / \{1 + \exp[(V + 53.3)/14.54]\}^4$, $\tau_B = 1.24 + 2.678 / \{1 + \exp[(V + 50)/16.027]\}$. The maximal conductance is

$g_A = 9.54$ μ S and the reversal potential is $V_A = -75$ mV. The steady-state value of the conductance $g_A A_\infty^3 B_\infty$ is nonzero over a large voltage range and the current I_A contributes a significant outward current above its reversal potential. The high reversal potential of the leak current $V_L = -17$ mV is chosen such that the resting potential of the model neuron is -68 mV.

PYRAMIDAL CELL. In contrast with fast-spiking interneurons, pyramidal cells are characterized by pronounced spike-frequency adaptation. A two compartment model with a total surface area of 0.05 mm² (the surface area for soma and dendrite is 0.025 mm² each) accounts for adaptation properties of pyramidal cells (Wang 1998). The voltage balance equations for the soma and dendrites are, respectively

$$\begin{aligned} C_m dV_s/dt &= -I_L - I_{Na} - I_K - (g/p)(V_s - V_d) - I_{syn} + I_{ext} \\ C_m dV_d/dt &= -I_L - I_{Ca} - I_{AHP} - [g_c/(1-p)](V_d - V_s) \end{aligned} \quad (3)$$

The capacitance of the membrane is $C_m = 0.25$ nF. The dynamics of the leak current I_L and the spike generating currents I_{Na} and I_K are the same as those given for the interneuron except $\alpha_h = 0.07 \exp[-0.1(V + 50)]$, $\beta_h = 1.0 / \{\exp[-0.1(V + 20)] + 1\}$ and $\alpha_m(V) = -0.1(V + 33) / \{\exp[-0.1(V + 33)] - 1\}$ and $\beta_m(V) = 4 \exp[-(V + 58)/12]$. The maximal conductances are $g_L = 0.025$ μ S, $g_{Na} = 11.25$ μ S and $g_K = 4.5$ μ S. The reversal potentials are $V_L = -65$ mV, $V_{Na} = 55$ mV and $V_K = -80$ mV. The temperature factors are $\phi_n = \phi_h = 4$. The high-threshold calcium current in the dendrite $I_{Ca} = g_{Ca} m_\infty^2 (V - V_{Ca})$, where m is assumed fast and is replaced by its steady state $m_\infty = 1 / \{1 + \exp[-(V + 20)/9]\}$. The maximal conductances are $g_{Ca} = 0.25$ μ S and the reversal potential is $V_{Ca} = 120$ mV. The voltage-dependent, calcium-activated potassium current $I_{AHP} = g_{AHP} [Ca^{2+}] / ([Ca^{2+}] + K_d) (V - V_K)$ with $K_d = 30$ μ M. The intracellular calcium follows $[Ca^{2+}]/dt = -\alpha I_{Ca} - [Ca^{2+}] / \tau_{Ca}$, where $\alpha = 4$ μ M/(ms \cdot μ A) and $\tau_{Ca} = 80$ ms. The maximal conductance $g_{AHP} = 1.25$ μ S.

EXPONENTIAL INTEGRATE-AND-FIRE MODEL. Fourcaud-Trocmé et al. (2003) recently showed that a simplified model, the exponential integrate-and-fire (EIF) model, can accurately reproduce the dynamics of the Wang and Buzsáki (1996) model. The advantage of this model is that its response to oscillatory input at high frequencies can be computed analytically (Fourcaud-Trocmé et al. 2003). The dynamics of the model is described by

$$C_m dV/dt = -g_L [V - V_L - \Delta_T e^{(V - V_m)/\Delta_T}] + I_{syn} + I_{ext} \quad (4)$$

where $C_m = 0.2$ nF, the leak conductance $g_L = 0.02$ μ S, the resting potential $V_L = -67$ mV and I_{syn} is the synaptic current and I_{ext} is an external applied current. The exponential term represents a simplified “fast sodium current” responsible for spike initiation. The parameters of this current are chosen so that its firing rate–current relationship is identical to that of the conductance-based interneuron model (Wang and Buzsáki 1996) for currents close to the current threshold. This gives $V_{th} = -62.45$ mV and $\Delta_T = 3.48$ mV. The reset potential $V_{reset} = -70.2$ mV and the refractory period of 1.4 ms are chosen so that the firing rate–current relationship also matches closely for large input currents.

Single-cell studies

INPUT CURRENT. Firing rate responses of single cells are computed following Brunel et al. (2001). A conductance-based single neuron receives an input current $I(t)$, which mimics the synaptic plus external input $[I_{syn}(t) + I_{ext}(t)]$. The current $I(t) = I_0 + I_1 \cos(2\pi ft) + I_{noise}$ such that the current $I(t)$ oscillates around a mean I_0 with frequency f and amplitude I_1 . The noise current is modeled as low-pass-filtered Gaussian white noise $dI_{noise}/dt = [\eta(t) - I_{noise}] / \tau_{noise}$ where $\eta(t)$ is a Gaussian white-noise random variable with zero mean and SD σ_{noise} chosen so that the SD of the subthreshold membrane potential is $\sigma_v =$

5 mV, which is comparable with physiological data (Destexhe and Paré 1999). The time constant $\tau_{noise} = 0-40$ ms. This noisy input yields a highly irregular single neuron spike train, in all cases investigated in this paper. The instantaneous firing rate of the neuron (instantaneous probability of emitting a spike per unit time) is averaged over 3,000 trials and the function $r(t) = r_0 + r_1(f) \cos[2\pi ft + \phi_{cell}(f)]$ is fitted to it using a least-square fit, where r_0 is the mean firing rate, $r_1(f)$ is the amplitude of the modulation, f is the frequency of the input current, and $\phi_{cell}(f)$ is the phase shift between the input current and the output firing rate. The mean (I_0) and amplitude (I_1) of the input current are chosen so that $r_1(f)/r_0 = 0.9$ at $f = 1$ Hz. The length of each trial (2 s) allows a fit over at least two periods of the oscillatory input. With I_0 and I_1 fixed, the normalized amplitude $r_1(f)/[r_1(f = 1 \text{ Hz})]$ and the phase shift $\phi_{cell}(f)$ of the instantaneous firing rate are computed for different frequencies f .

EFFECTIVE MEMBRANE TIME CONSTANT. Synaptic input modulates the membrane conductance and therefore the membrane time constant. The membrane time constant determines how fast the membrane can integrate synaptic input, and it can be used as a measure to characterize the membrane dynamics. The effective membrane time constant is defined as the inverse of the total conductance of the cell $\tau_{m-eff}(t) = C_m/[g_L + g_{ion}(t) + g_{syn}(t)]$, where g_{ion} is the total conductance including all ionic currents and g_{syn} is the sum over all synaptic conductances. In the noise-dominated regime, when the oscillation amplitude of the conductance is small, we approximate the effective membrane time constant by its time average. We exclude the spikes by excluding the conductances of the spike-generating sodium and potassium currents, which contribute to the total conductance significantly only during the spike and are small otherwise compared to the synaptic conductance

$$\tau_{m-eff} = \langle C_m/[g_L + \bar{g}_{ion} + g_{syn}(t)] \rangle_t \quad (5)$$

where \bar{g}_{ion} is the sum of all ionic conductances *excluding* the spike-generating sodium and potassium conductances and $\langle \cdot \rangle_t$ denotes the time average. In the case of single-cell simulations where we add a shunting conductance to mimic synaptic input, the effective membrane time constant for the conductance-based interneuron used here is simply

$$\tau_{m-eff} = C_m/(g_L + g_{shunt}) \quad (6)$$

Network simulations

NETWORK ARCHITECTURE. Network simulations are carried out with either one population of $N_I = 1,000$ interneurons, or two populations of $N_I = 1,000$ interneurons and $N_P = 4,000$ pyramidal cells. The architecture of the network is that of a sparsely and randomly directed graph: for each neuron pair, the connection probability is 10% in either direction, except in Fig. 7 where the connectivity is 5%. Thus on average, with a connectivity of $p = 10\%$ a given cell receives $M_F = pN_I = 100$ inhibitory synapses, and (in a two-population network) $M_P = pN_P = 400$ excitatory synapses.

SYNAPTIC CURRENTS. The synaptic currents are described by $I_{syn} = g_{syn}s(t)(V - V_{syn})$, where g_{syn} is the synaptic conductance, $s(t)$ is the fraction of open channels at time t , and V_{syn} is the reversal potential. The time course of $s(t)$ is faster for α -amino-3-hydroxy-5-methyl-4-isoxazolepropionic acid (AMPA)-mediated excitation than for GABAergic inhibition and can be characterized by the three time constants: synaptic latency (τ_i), rise time (τ_r), and decay time (τ_d)

$$s(t) = \exp\left[-\frac{(t - \tau_i)}{\tau_d}\right] - \exp\left[-\frac{(t - \tau_i)}{\tau_r}\right] \quad \text{for } t > \tau_i \quad (7)$$

where the time $t = 0$ corresponds to the voltage maximum of the presynaptic spike. The peak conductance is given by $\bar{g}_{syn} = g_{syn}(\tau_r/\tau_d)^{\tau_r/(\tau_r - \tau_d)}(1 - \tau_r/\tau_d)$. The synaptic conductances are chosen such that

the postsynaptic potential has an amplitude of 1 mV at a holding potential of -60 mV for pyramidal cells and -63 mV for interneurons just below threshold (Buhl et al. 1997; Markram et al. 1997; Tamas et al. 1997, 1998; Vida et al. 1998) and such that the ratio of the peak conductance $\bar{g}_{GABA_A}/\bar{g}_{AMPA} \approx 7.5$ (Bartos et al. 2001, 2002; Gupta et al. 2000; Markram et al. 1997). The time constants for AMPA are $\tau_{PI} = 1.5$ ms, $\tau_{Pr} = 0.5$ ms, and $\tau_{Pd} = 2$ ms (Angulo et al. 1999; Zhou and Hablitz 1998). For γ -aminobutyric acid type A (GABA_A) they are $\tau_{I1} = 0.5$ ms, $\tau_{Ir} = 0.5$ ms and $\tau_{Id} = 5$ ms (Bartos et al. 2001; Gupta et al. 2000; Kraushaar and Jonas 2000; Xiang et al. 1998). The reversal potential of AMPA is $V_{syn,AMPA} = 0$ mV and of GABA_A $V_{syn,GABA_A} = -75$ mV. The peak conductances are $\bar{g}_{AMPA \rightarrow P} = 1.3$ nS, $\bar{g}_{GABA \rightarrow P} = 8.75$ nS, $\bar{g}_{AMPA \rightarrow I} = 0.93$ nS, and $\bar{g}_{GABA \rightarrow I} = 6.2$ nS.

EXTERNAL INPUTS. Each neuron receives external synaptic input, modeled as a high-frequency Poisson spike train with a rate λ . The external input is mediated by AMPA synapses with conductances of 15.8 nS in pyramidal cells and 1.5 nS in interneurons. In Fig. 10 we used additional external inhibitory GABAergic input to interneurons with a conductance of 8.8 nS.

THE INSTANTANEOUS FIRING RATE. The spike times from all neurons are binned in a sliding window with $\Delta t = 0.2$ ms. The spike times are taken at the voltage maximum. The instantaneous firing rate at time t , $r(t)$, is then the number of spikes in the time window $[t, t + \Delta t]$, divided by the number of neurons and by Δt .

MEASURE OF SYNCHRONY. To characterize the synchrony in the network we compute the autocorrelation function of the instantaneous population firing rate, normalized by the square of the average rate. In all cases described herein, the autocorrelation function is well described by a damped cosine function, with a narrow peak at the zero time lag bin, which is ascribed to the finite size of the network. To remove this finite size effect, we fit the autocorrelation function with a damped cosine, excluding the zero time lag bin. The measure of synchrony is the value of the damped cosine that best fits the data at zero time lag. This measure quantifies how much spike trains of different neurons are correlated.

Single spike train

SPECTRUM AND AUTOCORRELATION FUNCTION. To analyze the rhythmicity of a single spike train during network oscillations we calculate the power spectrum and autocorrelation function of one single spike train and of the combined spikes of a group of cells (Gabbiani and Koch 1998). The representative spike trains are selected randomly from the neural population.

SPIKE-TRIGGERED AVERAGE (STA) OF GLOBAL ACTIVITY. The spike triggered average is the cross-correlation between the spike train of a single neuron and the global activity. The instantaneous firing rate of a population during a 300-ms time window surrounding a spike (150 ms before and 150 ms after the spike time) is averaged over all spikes of the spike train of a single neuron.

Numerical methods

All equations are computed using a scheme based on the Runge-Kutta algorithm (fourth order for the network and second order for the single cell simulations) to solve the coupled differential equations (Press et al. 1992). Integration time step is $\Delta t = 0.02$ ms.

RESULTS

Response of a single cell to noisy sinusoidal current

The transformation of the incoming synaptic inputs into an output spike train by single neurons is classically described in

terms of a current–frequency relationship. However, the prediction of the collective response of a neuronal population to time-varying inputs requires a more detailed characterization of the firing properties of single cells. A standard procedure when dealing with nonstationary inputs is to characterize neurons by the *linear firing rate response*, i.e., the instantaneous firing rate response to noisy inputs with a weak sinusoidal modulation at an arbitrary frequency f (see e.g. Brunel et al. 2001; Gerstner 2000; Knight 1972). The idea is that during a network oscillation at frequency f , the combined external and recurrent synaptic current in a neuron can be modeled as a high-frequency inhomogeneous Poisson process, which is approximately described as

$$I(t) = I_0 + I_1 \cos(\omega t) + I_{noise} \quad (8)$$

where I_0 is a constant mean current and I_1 is the amplitude of the modulation at frequency $f = \omega/2\pi$ (see METHODS). Fluctuations arising from random arrival of spikes can be well approximated by low-pass-filtered Gaussian white noise with a time constant τ_{noise} (corresponding to the synaptic decay time constant). The neuron's response to such a current can be characterized by its instantaneous firing rate $r(t)$, obtained by an average of the response over many trials (Fig. 1A). The instantaneous firing rate follows the current with a phase shift $\phi_{cell}(\omega)$

$$r(t) = r_0 + r_1(\omega) \cos[\omega t + \phi_{cell}(\omega)] \quad (9)$$

This linear approximation is valid for small enough I_1 and, in particular, for the values of I_1 used in Fig. 1, A and B, as shown in Fig. 2 for several representative frequencies. The amplitude of the modulation $r_1(\omega)$ and the phase $\phi_{cell}(\omega)$ depend on the frequency f of the input current. We compute the normalized amplitude $r_1(\omega)/[r_1(f = 1 \text{ Hz})]$ and the phase $\phi_{cell}(\omega)$ for different values of the frequency f , whereas all other parameters in the input current remain unchanged. Here, we use the convention that a *negative* phase corresponds to a *late* firing in the oscillatory cycle. In simulations, the mean current I_0 is adjusted such that the mean firing rate is fixed ($r_0 = 40 \text{ Hz}$), so that the rate r_0 does not depend on the input frequencies f . The amplitude I_1 is chosen so that $r_1(f)/r_0 = 0.9$ at $f = 1 \text{ Hz}$ input frequency and $r(t)$ is always nonzero.

It has been shown for LIF neurons that the response of a neuron to a noisy sinusoidal current strongly depends on the time constant of the noise τ_{noise} (Brunel et al. 2001 and Fig. 1C). The phase lag decreases and the amplitude increases for larger noise time constants. When the time constant τ_{noise} is sufficiently large, the LIF model responds to sinusoidal input superimposed on synaptically filtered noise with negligible phase shift, independent of the input frequency. This salient feature of the LIF model neuron is crucial for neurons to follow fast transients and to enable a network of LIF inhibitory neurons to generate very fast (up to 300 Hz) coherent oscillations (Brunel and Wang 2003; Brunel et al. 2001).

In sharp contrast to the LIF neuron, we found that a conductance-based neuron responds to the noisy oscillating current with a phase lag that depends very weakly on the time constant of the noise (Fig. 1B). The phase and amplitude behave essentially in the same way whether the input is Gaussian white noise ($\tau_{noise} = 0 \text{ ms}$) or filtered with a large time constant ($\tau_{noise} = 40 \text{ ms}$) (Fig. 1B). When the input current varies slowly so that f is well below the average firing rate r_0 , the

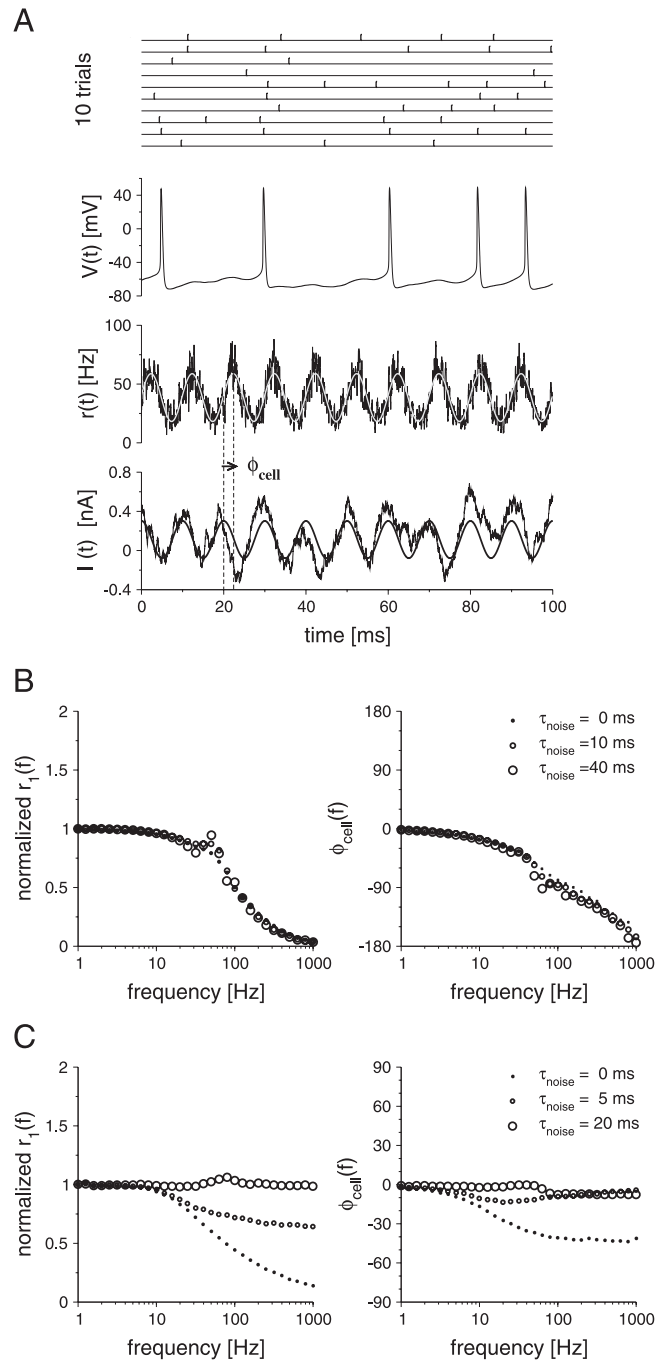


FIG. 1. Firing properties of a single model neuron in response to a noisy sinusoidal input current. A: response of a single cell to 100-Hz oscillations: noisy sinusoidal current (the smooth curve is the deterministic part of the current) occasionally induces spikes, as shown in the membrane potential $V(t)$ trace. Instantaneous firing rate $r(t)$, averaged over 3,000 trials, oscillates at 100 Hz but is phase shifted by ϕ_{cell} [the smooth curve is the least-square fit to the function $r(t) = r_0 + r_1 \cos(\omega t + \phi_{cell})$]. Top: spike raster of 10 trials (time constant of the noise is $\tau_{noise} = 5 \text{ ms}$, the average firing rate is 40 Hz, $I_0 = 0.12 \text{ pA}$, and $I_1 = 0.175 \text{ pA}$). B: phase and normalized amplitude of the trial-averaged firing rate, as a function of input frequency for conductance-based neurons. Phase and normalized amplitude depend only weakly on the time constant of the noise (τ_{noise}). Normalized amplitude of the rate $r_1(\omega)/r_1(f = 1 \text{ Hz})$ (left) and the phase shift ϕ_{cell} (right) decrease with increasing frequency of the input current. C: phase and normalized amplitude as a function of frequency for leaky integrate-and-fire (LIF) neurons. Phase and normalized amplitude depend on the time constant of the noise (τ_{noise}). When τ_{noise} is sufficiently large, the LIF model neurons respond to the noisy sinusoidal input current without attenuation (left) and without a phase lag (right). Note that a *negative* phase corresponds to *late* firing during the oscillatory cycle.

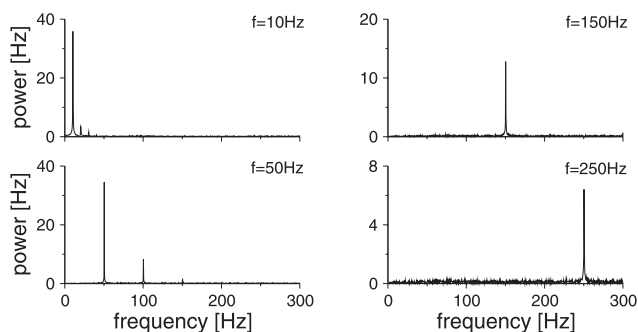


FIG. 2. Power spectrum of the averaged firing rate $r(t)$ is clearly dominated by a sharp peak at the input frequency f . Instantaneous firing rate of a neuron responding to a noisy sinusoidal current with frequency $f = 10, 50, 150$, and 250 Hz, respectively, is averaged over 3,000 trials. Mean firing rate of the neuron is 40 Hz. I_0 and I_1 are the same as in Fig. 1.

response of the cell follows the modulation without a phase lag and the oscillation amplitude stays constant. For larger frequencies $f > r_0$, the firing rate lags behind the current with a phase lag $\phi_{cell}(\omega)$ and the amplitude of the modulation $r_1(\omega)$ decreases. For example, at $f = 100$ Hz the instantaneous firing rate $r(t)$ lags behind the current by about $\phi_{cell} = -90^\circ$, whereas the averaged firing rate $r_0 = 40$ Hz is constant for all input frequencies f (Fig. 1B). The neuron acts as a low-pass filter.

A more quantitative description of the phase shift $\phi_{cell}(\omega)$ can be achieved by fitting a function to the simulation data that captures the important features of the response. We find that the phase shift $\phi_{cell}(\omega)$ as a function of the frequency of the input current $f = \omega/2\pi$ can be well described by a function of the form (see Fig. 3A)

$$\phi_{cell}(\omega) = -\omega\tau_{spike} - \text{atan}(\omega\tau_{filter}) \quad (10)$$

The first term on the right-hand side of Eq. 10 is a constant delay arising from the finite spike time to peak (see Fig. 3B). After the membrane potential has reached a certain depolarization threshold (about -45 mV), the membrane dynamics is dominated by the Na^+ and K^+ currents and is largely independent of the fluctuations in the input current. Thus the shape of the spike is independent of the inputs. The constant delay τ_{spike} corresponds to the time to peak of the action potential, that is, the time it takes from the point when the spike is already well initiated to the voltage maximum where the spike time is defined. The second term is related to the voltage dynamics near spike initiation and below the depolarization threshold. It can be well described by a linear filter with time constant τ_{filter} and is best understood in the context of the simplified EIF neuron (see below). In the example given in Fig. 3 we found that $\tau_{spike} = 0.24$ ms and filter time constant $\tau_{filter} = 4$ ms.

How do these two time constants τ_{filter} and τ_{spike} depend on the properties of the neuron? As already mentioned, τ_{spike} depends exclusively on the interplay of the Hodgkin–Huxley currents leading to spike generation, independently of the inputs. On the other hand, τ_{filter} does depend on the synaptic inputs. Our single-cell simulations allow us to identify two crucial parameters that control τ_{filter} : the single-cell mean firing rate and the input conductance.

MEAN FIRING RATE. We computed the phase shift $\phi_{cell}(\omega)$ as a function of the input frequency f for different mean firing rates r_0 . Different single-cell firing rates are achieved by adjusting

the mean input current I_0 . Simulations show that the phase shift depends substantially on the average firing rate of the single cells (Fig. 4A). The filter time constant τ_{filter} decreases with increasing mean firing rate, whereas τ_{spike} is independent of r_0 (Fig. 4B). The instantaneous firing rate follows the input current with a smaller phase lag for larger average firing rates.

INPUT CONDUCTANCE. Synaptic inputs as well as intrinsic currents that are active in the subthreshold voltage range introduce changes in the input conductance of the neuron. If the fluctuations in the conductance are small, the synaptic conductance can be approximated by a constant term. Thus we introduce a shunting term into the input current that mimics the total synaptic conductance (external and recurrent) during network activity. This allows us to vary the neuron's input conductance and, equivalently, the neuron's effective membrane time constant τ_{m-eff} (see also Eq. 6)

$$I(t) = I_0 + I_1 \cos(\omega t) + I_{noise} - g_{shunt}(V - V_L) \quad (11)$$

For different values of g_{shunt} we adjust the SD of σ_{noise} so that the fluctuations in the membrane potential are kept at about $\sigma_V = 5$ mV. As shown in Fig. 4C the addition of a shunting conductance g_{shunt} leads to a reduction in the cellular phase lag $\phi_{cell}(\omega)$ in the firing response to a noisy sinusoidal input. The time constant characterizing the spike time to peak τ_{spike} is unaffected by changes in g_{shunt} and the changes in $\phi_{cell}(\omega)$ are attributed entirely to changes in τ_{filter} (Fig. 4D). A small effective membrane time constant leads to a smaller phase lag and allows the neuron to follow high-frequency inputs better.

The exponential integrate-and-fire neuron

Are the results presented in the previous section specific to models with Hodgkin–Huxley mechanisms or can they be obtained with a simpler integrate-and-fire-like model? The exponential integrate-and-fire (EIF) model (see METHODS) was recently introduced to incorporate the dynamics of spike initiation in the LIF model (Fourcaud-Trocmé et al. 2003). In the EIF model, the activation kinetics of the fast sodium current is assumed instantaneous and the voltage-dependent activation voltage dependency is assumed to be exponential (controlled by the parameter Δ_T , Eq. 4). The EIF model does not include

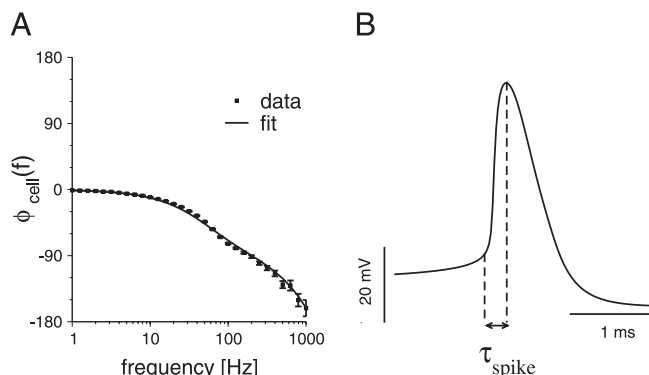


FIG. 3. Phase shift curve fitted by a simple delayed filter. A: single-cell simulations (full squares) and the fitted function (solid curve). Function fitted to the data is $-360f\tau_{spike} - (180/\pi) \text{atan}(2\pi f\tau_{filter})$, with $\tau_{spike} = 0.24$ ms and $\tau_{filter} = 4.0$ ms. Single-cell firing rate is 40 Hz; the synaptic time constant $\tau_{noise} = 5$ ms; SD of the noise is $\sigma_{noise} = 5$ mV. B: interpretation of fixed delay τ_{spike} : spike time to peak is the time from threshold to the maximum of the spike. For the conductance-based interneuron (see METHODS) $\tau_{spike} = 0.24$ ms.

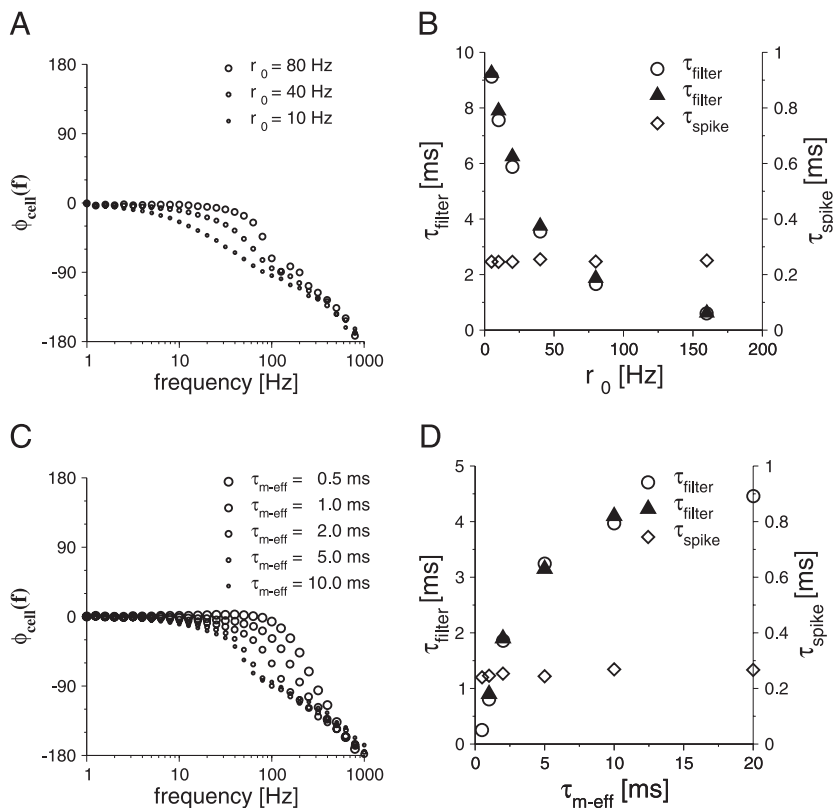


FIG. 4. Dependency of the phase shift on membrane time constant and mean firing rate. *A*: single-cell phase shift $\phi_{cell}(\omega)$ decreases with increasing single-cell mean firing rate r_0 at high frequencies. Firing rate is increased by increasing the mean current I_0 . *B*: intrinsic time constant τ_{filter} decreases with increasing r_0 . Filled triangles are τ_{filter} calculated from the asymptotic behavior of the exponential integrate-and-fire (EIF) neuron and the gain of the r_0 - I curve $\tau_{filter} = (C_m \Delta_T dr_0/dI)/r_0$. Delay τ_{spike} is not affected by r_0 . Effective membrane time constant is $\tau_{m-eff} = 10$ ms. *C*: single-cell firing rate phase shift $\phi_{cell}(\omega)$ decreases with increasing shunting conductance at high frequencies. *D*: intrinsic time constant τ_{filter} (obtained by fitting the phase data in *A* with Eq. 10) decreases with $\tau_{m-eff} = C_m/(g_L + g_{shunt})$. Filled triangles are τ_{filter} calculated from the asymptotic behavior of the EIF neuron and the gain of the r_0 - I curve $\tau_{filter} = (C_m \Delta_T dr_0/dI)/r_0$. Delay τ_{spike} is not affected by τ_{m-eff} . The slope dr_0/dI is computed numerically. Single-cell firing rate is $r_0 = 40$ Hz.

the repolarizing mechanism of the potassium current but, instead, the voltage is set to a reset potential after reaching a set peak value. The parameters of the EIF model neuron are chosen such that the firing rate–current relationships of the EIF and the conductance-based model neurons are almost indistinguishable (Fig. 5*B*), as are the voltage traces in response to noisy currents, except for a short interval after spike initiation (Fig. 5*A* and Fourcaud-Trocmé et al. 2003).

The linear response of the EIF model neuron was obtained in the same way as for the conductance-based model (see previous section and METHODS). Simulations show that the single cell’s response to the noisy sinusoidal current is essentially independent of the time constant of the noise τ_{noise} (Fourcaud-Trocmé et al. 2003), as it is for the conductance-based model. As shown analytically by Fourcaud-Trocmé et al. (2003), the phase shift $\phi_{cell}(f)$ goes to 90° for large input frequencies f . Indeed, Fig. 5*C* shows that, in addition, the phase shift can be well fitted with an arctangent function (Eq. 10). The time constants τ_{spike} and τ_{filter} are taken from a fit with the function in Eq. 10 to the simulated data. The fact that the phase goes to 90° at large frequencies implies that for the EIF model $\tau_{spike} = 0$. The remaining term is the low-pass filter with time constant τ_{filter} . The values of τ_{filter} for different shunt conductances, or equivalently for different τ_{m-eff} are similar to those of the conductance-based model (compare Figs. 4*C* and 5*C*). Thus, all the results obtained with the conductance-based models can be reproduced quantitatively by the simpler EIF model. The use of the simpler model confirms that the phase shift in the single cell response arises from the dynamics of the spike initiation that is well captured by the exponential term of the EIF, and that the effective membrane time constant has a major influence on the single-cell phase shift.

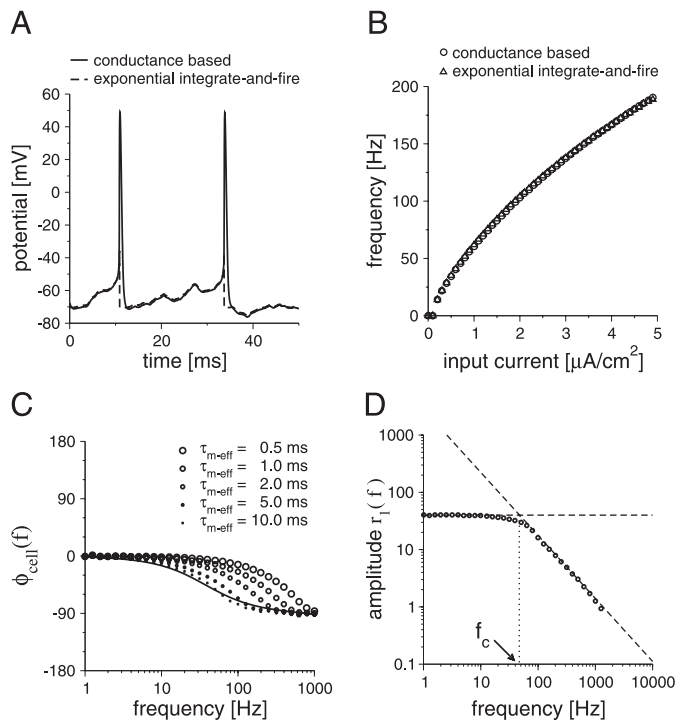


FIG. 5. EIF model reproduces quantitatively the behavior of a conductance-based model neuron. *A*: subthreshold potentials of conductance-based and EIF neurons match well with each other, except for a short time interval right after the spike discharge. *B*: parameters of the EIF neuron can be chosen such that the r_0 - I curves of the EIF model neuron and conductance-based neuron are comparable. *C*: phase of the single cell’s response to noisy sinusoidal current input depends on the effective membrane time constant τ_{m-eff} and can be fitted by a linear filter. Smooth curve is $-\text{atan}(2\pi f \tau_{filter})$, where $\tau_{filter} = 4$ ms. *D*: time constant τ_{filter} can be estimated from the cutoff frequency f_c , defined as the intersection between the low- and high-frequency limits of the response amplitude (also see text).

A simple analytical estimate of τ_{filter} for the EIF model neuron can be obtained from the low- and high-frequency limits investigated by Fourcaud-Trocmé et al. (2003) (see also Fig. 5D). In the low-frequency range, the linear response amplitude is essentially constant and proportional to the gain of the r_0 - I curve at the corresponding mean frequency, i.e., dr_0/dI . In the high-frequency range, the amplitude decays as $r_0/(C_m\Delta_T 2\pi f)$. This behavior is reminiscent of a simple low-pass-filter rate model of the type $\tau dr/dt = -r + \phi[I(t)]$. For such a rate model, in response to a sinusoidal input, the amplitude of the firing rate modulation decays with f as $r_1(f) \sim 1/\sqrt{[1+(f/f_c)^2]}$, and the phase shift of the rate modulation is $\text{atan}(ff_c)$, where the cutoff frequency is related to the time constant τ of the rate model by $f_c = 1/(2\pi\tau)$. For such a rate model, the cutoff frequency corresponds to the frequency at which the asymptotic expressions for $r_1(f)$ in the low ($r_1 \sim 1$) and high ($r_1 \sim f_c/f$) frequency limits are equal. We can define the cutoff frequency in a similar way for the EIF model, which gives $f_c = r_0/(2\pi C_m \Delta_T dr_0/dI)$ (Fig. 5D). This in turn gives an estimate of the filter time constant, $\tau_{filter} = 1/(2\pi f_c)$, or $\tau_{filter} = (C_m \Delta_T dr_0/dI)/r_0$. This estimate turns out to be very close to the one obtained by the fitting procedure, as shown in Figs. 4, B and D. Note that one deduces directly from the analytical formula that the filter time constant decreases when the firing rate increases. Furthermore, it shows that the filter time constant is also proportional to the slope (gain) of the r_0 - I curve, and to the spike activation parameter Δ_T . The input conductance affects τ_{filter} through its effect on the slope of the r_0 - I curve (not shown) (Chance et al. 2002). In the high-noise regime considered here, increasing input conductance *decreases* the gain of the r_0 - I curve, when the mean firing rate is maintained constant. As a result, the filter time constant is decreased.

To summarize the single cell results, we found that, unlike the LIF model, the firing-rate response of a conductance-based model neuron to synaptically filtered noisy sinusoidal input is highly dependent on the input frequency. The phase shift in the firing rate can be described as the sum of two terms: the near-threshold voltage dynamics give rise to a filter term with τ_{filter} and the threshold-to-peak spike width leads to an intrinsic latency τ_{spike} . The time constant τ_{filter} is highly dependent on the effective membrane time constant and mean firing rate, whereas τ_{spike} is not. Unlike LIF neurons, which can follow fast transients, the response of conductance-based neurons is strongly dependent on the single cell firing rate and the input conductance. The response properties of the conductance-based neuron can be well captured by the EIF neuron.

Theoretical determination of the population frequency of a network of inhibitory neurons

We now incorporate the response properties of single neurons in a theoretical framework that allows us to determine quantitatively the frequency of network oscillations. This represents an extension of the analysis of Brunel and Wang (2003), which assumed that single neurons respond instantaneously to inputs at all frequencies. To start with, we assume that during collective oscillatory population activity, the averaged instantaneous firing rate $r_i(t)$ can be roughly described as a sinusoidal function. Single cells fire irregularly in time with a discharge probability equal to this sinusoidal function.

Thus, the activity of each neuron in the population can be described by

$$r_i(t) = r_{i,0}[1 + \nu \cos(\omega t)] \quad (12)$$

where $r_{i,0}$ is the mean firing rate of the cell, $\nu = r_{i,1}/r_{i,0}$ is the relative amplitude of the sinusoidal modulation in the firing rate, and $\omega = f/2\pi$, where f is the frequency of the sinusoidal modulation and corresponds to the population frequency (Figs. 1A and 6), yet to be calculated.

First, we consider the time course of GABAergic currents in the inhibitory neurons of the network. A sinusoidally varying presynaptic firing rate leads to the average fraction of open channels at GABAergic synapses varying as a sinusoidal function of time. However, because of temporal characteristics (latency τ_{lb} , rise time τ_{lr} and decay time τ_{ld}) of GABAergic synapses, there is a phase shift of the time course of the fraction of open channels with respect to the presynaptic firing rate. For synapses described by Eq. 7 this phase shift $\phi_{l,syn}(\omega)$ is given by (Brunel and Wang 2003)

$$\phi_{l,syn}(\omega) = -\omega\tau_{ll} - \text{atan}(\omega\tau_{lr}) - \text{atan}(\omega\tau_{ld}) \quad (13)$$

Note that a negative phase shift corresponds to a phase lag. The synaptic current is the product of the fraction of open channels at GABAergic synapses multiplied by the driving force. Assuming that the temporal variations in the driving force are small compared to the temporal variations in the fraction of open channels, the phase shift of the GABAergic current is given by $\phi_{l,syn}(\omega) - \pi$, where the factor π comes from the inhibitory nature of GABAergic currents.

The next step is to determine the time course of the firing rate of a postsynaptic neuron that receives an oscillatory current with a phase shift $\phi_{l,syn}(\omega) - \pi$. We have seen in the previous section that such a postsynaptic neuron will respond to a noisy sinusoidal current with a phase shift $\phi_{l,cell}(\omega)$, which also depends on the input frequency f . Thus the total phase shift of the postsynaptic firing rate with respect to the presynaptic one is $\phi_{l,syn}(\omega) - \pi + \phi_{l,cell}(\omega)$. Because the instantaneous firing rate of pre- and postsynaptic neurons must be in phase for network oscillations to emerge, this total phase shift must be equal to -2π , i.e.

$$\begin{aligned} -\pi &= \phi_{l,syn}(\omega) + \phi_{l,cell}(\omega) \\ &= -\omega\tau_{ll} - \text{atan}(\omega\tau_{lr}) - \text{atan}(\omega\tau_{ld}) + \phi_{l,cell}(\omega) \end{aligned} \quad (14)$$

Equation 14 gives the predicted population frequency. It shows that long synaptic time constants increase the phase and decrease the population frequency (see also Brunel and Wang 2003). When the phase shift arising from the single-cell response is negligible as in the case of LIF neurons, $\phi_{l,cell}(\omega) = 0$, the population frequency can be computed by solving the equation $\pi = \omega\tau_{ll} + \text{atan}(\omega\tau_{lr}) + \text{atan}(\omega\tau_{ld})$ (Brunel and Wang 2003). An additional phase lag [$\phi_{l,cell}(\omega) < 0$] reduces the population frequency as shown in Fig. 6B.

To obtain a prediction of the network frequency, we insert the phenomenological description of the phase shift $\phi_{l,cell}(\omega)$ of the single cell's response to noisy sinusoidal current (Eq. 10) in Eq. 14. The condition for the total phase in an oscillating network can then be written

$$\pi = \omega\tau_{ll} + \text{atan}(\omega\tau_{lr}) + \text{atan}(\omega\tau_{ld}) + \omega\tau_{l,spike} + \text{atan}(\omega\tau_{l,filter}) \quad (15)$$

Thus, the population frequency of a network of inhibitory

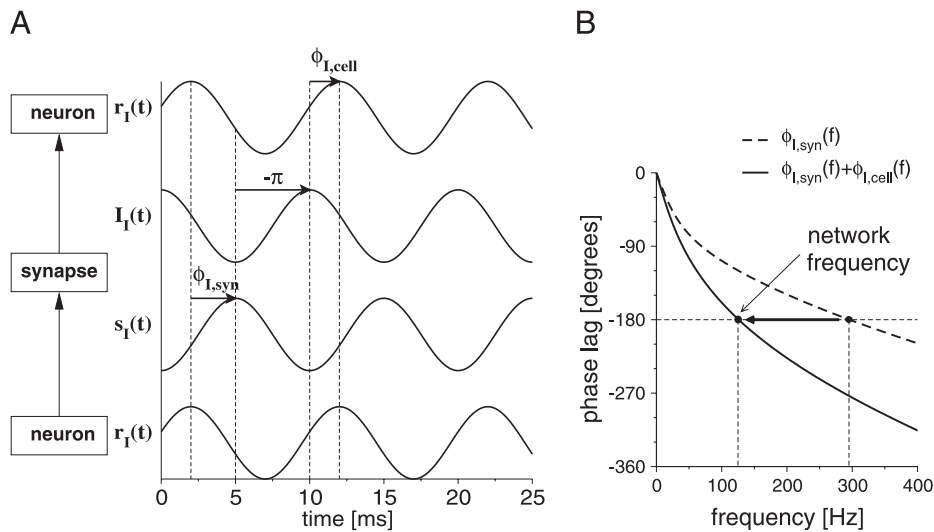


FIG. 6. Theoretical prediction of the rhythmic frequency of an interneuronal population. **A:** illustration of the analytical method. An inhibitory neuron has an average firing rate $r_I(t)$. Because of synaptic filtering, the fraction of open channels $s_I(t)$ lags behind the firing rate with a phase $\phi_{L,syn}(f)$. Synaptic current $I_I(t)$ is antiphasic to $s_I(t)$ because it is an inhibitory current. The neuron lags behind the synaptic current by $\phi_{L,cell}(f)$. For network oscillations to emerge the phase must satisfy $-\pi = \phi_{L,syn}(f) + \phi_{L,cell}(f)$, where f is the population frequency. **B:** total phase shift vs. frequency: population frequency is the intersection of the total phase shift [dashed line, synaptic phase $\phi_{L,syn}(f)$; solid line, synaptic + single-cell phase $\phi_{L,syn}(f) + \phi_{L,cell}(f)$] with the horizontal line at -180° . In the presence of synaptic filtering only, the population frequency is almost 300 Hz. Single-cell filtering reduces the population frequency to 125 Hz.

coupled neurons can be calculated by knowing the inhibitory synaptic time constants and the two cellular time constants $\tau_{I,spike}$ and $\tau_{I,filter}$. For example, when the phase shift is negligible for all input frequencies [$\phi_{L,cell}(f) \approx 0$, corresponding to LIF neurons], Eq. 15 predicts a population frequency of almost $f = 300$ Hz, assuming the standard synaptic time constants ($\tau_{II} = 0.5$ ms, $\tau_{Ir} = 0.5$ ms, $\tau_{Id} = 5.0$ ms). A delay $\tau_{I,spike} = 0.24$ ms corresponding to the spike time to peak lowers the population frequency to about $f = 230$ Hz. The single-cell filtering time constant $\tau_{I,filter}$ has a much stronger effect on the population frequency. For a firing rate of 40 Hz and an effective membrane time constant of 10 ms, we have seen in the previous section that $\tau_{I,filter} = 4$ ms. This leads to a decrease of the population frequency to $f = 95$ Hz. However, the effective membrane time constant is significantly reduced during network activity as a result of the synaptic conductance change and we expect a higher population frequency. For example, if the effective membrane time constant changes tenfold (from $\tau_{m-eff} = 10$ ms to $\tau_{m-eff} = 1$ ms) and the average firing rate of the neurons is $r_{I,0} = 40$ Hz we predict a population frequency $f \approx 140$ Hz.

Emergent oscillations in a population of conductance-based inhibitory interneurons

How does the analysis compare with simulation results? Simulations of a network composed of a single population of mutually connected inhibitory GABAergic Hodgkin–Huxley-type conductance-based cells show a prominent fast rhythm when the external drive is sufficiently large and recurrent inhibition is strong (Fig. 7A). A similar result was shown for a network of LIF neurons (Brunel and Wang 2003). During network activity single cells are subjected to synaptic currents, external excitation (Poisson rate λ of the AMPA-receptor-mediated synaptic inputs), and recurrent inhibition. The recurrent inhibition has an oscillatory component stemming from the emerging network oscillations. The synaptic inputs to each cell of the network induce a noisy subthreshold oscillation in the membrane voltage; fluctuations around the average subthreshold time course of the voltage occasionally cause a cell to spike. The spike pattern differs from cell to cell and the single-cell firing rates are heterogeneous across the network

because external drive is Poisson and recurrent connections are random and sparse. The power spectrum of a single spike train does not indicate any rhythmicity (Fig. 7B), even though “multiunit” activity averaged over a group of 10 cells during the same time interval shows a peak in the power spectrum at 125 Hz (Fig. 7C). This narrow peak in the power spectrum indicates that the network activity is indeed dominated by a single frequency component. Similarly, the autocorrelation of a single spike train does not show an oscillatory pattern (Fig. 7D); thus oscillations are hardly apparent in a single cell’s spike train, because the probability of firing in any given cycle is small. On the other hand, the population firing rate, averaged over a large number of cells, clearly reveals the network oscillation at a much higher frequency than the averaged single cell firing rate (Fig. 7A). Although single cells do not discharge rhythmically, they fire at a preferred phase of the population oscillation, as can be seen in the cross-correlation between the spike train of a single cell and the population activity (spike-triggered average of the population firing rate, Fig. 7E).

The oscillation frequency of 125 Hz (Fig. 7A) can be predicted from the single-cell analysis in the following way. First, given the synaptic time constants the synaptic phase shift can be computed as a function of the population frequency $\phi_{L,syn}(\omega)$ (Eq. 13). The next step is to determine the single-cell phase shift $\phi_{L,cell}(\omega)$, which depends on the average single cell firing rate (40 Hz) and the effective membrane time constant. Each neuron receives on average an inhibitory input of 2 kHz [average single cell firing rate (40 Hz) multiplied by the number of connections (50)] and an excitatory input of 5 kHz. Considering the conductances of recurrent inhibition ($\bar{g}_{GABA \rightarrow I} = 6.2$ nS) and external excitation ($\bar{g}_{ext \rightarrow I} = 1.5$ nS) and the time constants of each synapse, the total synaptic conductance can be computed to be $0.11 \mu\text{S}$. The neuron has therefore an effective membrane time constant of 1.5 ms. Using a single cell with a shunt conductance of $0.11 \mu\text{S}$, the single-cell phase shift can be determined. The time constants $\tau_{I,filter} = 1.6$ ms and $\tau_{I,spike} = 0.24$ ms can be obtained with a fit to the phase shift. The last step is to evaluate the self-consistent solution (Eq. 15), which leads to a population frequency of 127 Hz, remarkably close to what we observe (125 Hz) in network simulations.

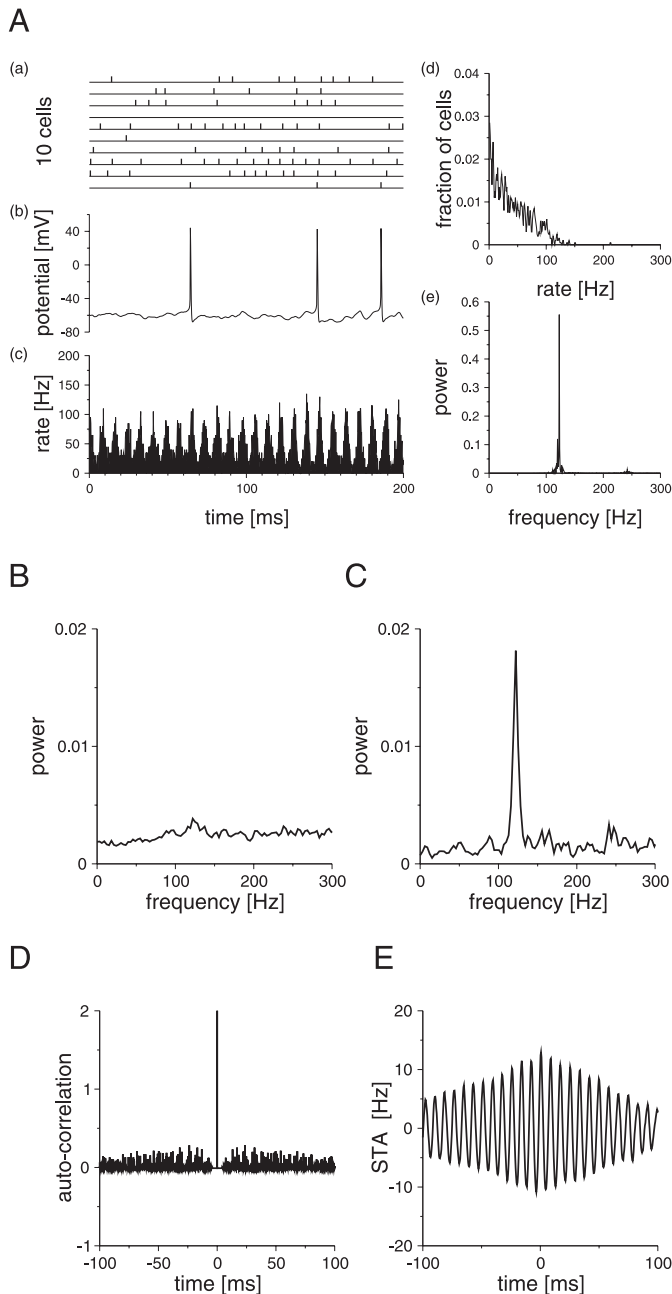


FIG. 7. Fast (>100 Hz) oscillations in a network of inhibitory neurons. *A*: single cells fire randomly and sparsely at a much lower frequency than the population activity. Network oscillations are apparent in the population activity rather than on the single-cell level. Network oscillates at 125 Hz, whereas the mean firing rate of single cells is 40 Hz: (a) spike raster of 10 cells; (b) membrane potential of a single cell; (c) instantaneous population firing rate; (d) distribution of single-cell firing rates across the population; (e) power spectrum of the instantaneous population firing rate. External excitatory input is 5 kHz. *B*: oscillations are not detectable with the power spectrum of single-cell spike trains (the single-cell spectrum is averaged over 10 cells). *C*: power spectrum of “multiunit” activity (combined spike trains from 10 cells) shows a clear peak at 125 Hz. *D*: autocorrelation of a single spike train does not show an oscillatory pattern. *E*: spike-triggered average (STA) of the population rate shows oscillations at 125 Hz. Spike-triggered population rate is averaged over the spikes of one neuron (42 spikes). Length of spike trains is 2 s. Parameters: connection probability 0.05; synaptic time constants for γ -aminobutyric acid (GABA) $\tau_{II} = 0.5$ ms, $\tau_{I'} = 0.5$ ms, $\tau_{Id} = 5.0$ ms.

How does the network frequency depend on the external excitation? The increase in external excitation leads to an increase in the single cell's firing rate and a decrease of the effective membrane time constant (resulting from increased external and recurrent synaptic conductance). Brunel and Wang (2003) showed that the oscillation frequency of a population of LIF neurons is independent of the external excitatory input because the response of the single LIF neuron to noisy oscillating synaptic current does not depend on the single-cell properties. In contrast, Fig. 8 shows that the conductance-based neuron's response to noisy oscillating synaptic current *does* depend on the single-cell properties. Indeed, when the external drive is varied gradually, the single-cell firing rate as well as the population frequency increase almost linearly. The population can oscillate at frequencies ranging from <100 to >200 Hz. This frequency range is significantly lower than the population frequency of a network of LIF model neurons (300 Hz), when the comparison is made with the same synaptic parameters (latency $\tau_{II} = 0.5$ ms, rise time $\tau_{I'} = 0.5$ ms, and decay time $\tau_{Id} = 5.0$ ms). Because the synaptic conductance affects the single-cell properties, and thus the phase shift with which the conductance-based neuron responds to the synaptic current, the population frequency of conductance-based neurons can be modulated by the synaptic afferents.

Role of membrane time constant of single neurons

An important conclusion from the single-cell study is that the effective membrane time constant of the single cell has a strong influence on the phase shift and therefore on the oscillation frequencies. We predict that fast oscillations can be obtained by a small single-cell effective membrane time constant. This raises the question as to whether physiologically observed frequencies of very fast oscillations (around 200 Hz) are realizable. We now discuss two possible scenarios by which a small effective membrane time constant might be obtained and, consequently, fast network oscillations might emerge. In the first scenario an intrinsic current activated in the subthreshold range is used, whereas in the second scenario large synaptic inputs lead to a decrease in the effective membrane time constant.

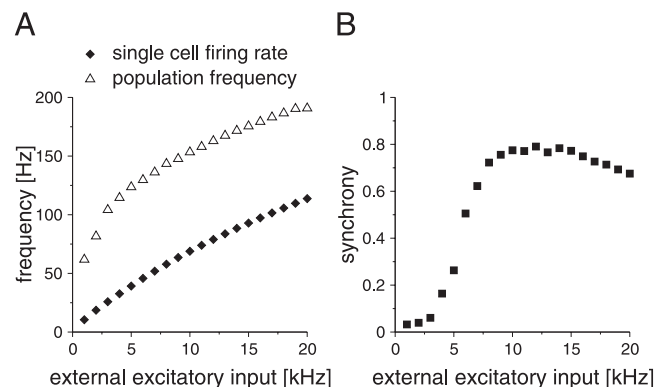


FIG. 8. Network oscillation frequency and neuronal firing rate as function of the input amplitude. *A*: population frequency increases with increasing input strength. Each cell receives an external excitatory Poisson input with rate λ . With increasing λ the single-cell frequency (filled diamonds; averaged over all cells) and the population frequency (triangles) increase. *B*: network synchrony increases rapidly when the input rate λ crosses a threshold (5 kHz) and saturates for larger input. Parameters as in Fig. 7.

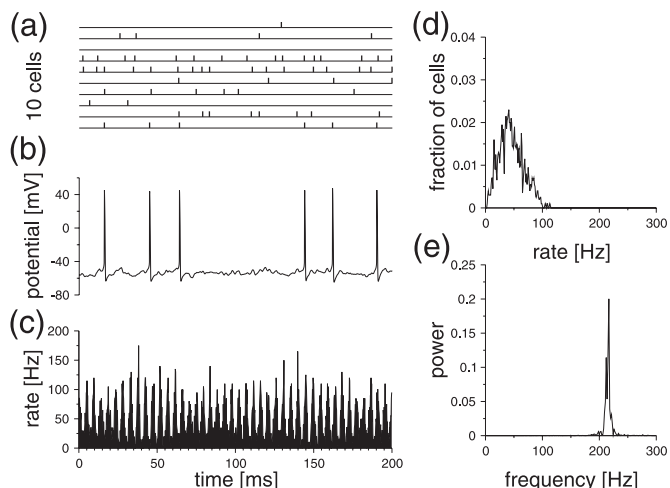


FIG. 9. A population of conductance-based neurons with a small effective membrane time constant can oscillate at 220 Hz. Single cells contain an A-type potassium current that contributes to reducing the effective membrane time constant at subthreshold potentials. During network activity, the membrane time constant $\tau_{m-eff} = 0.15$ ms: (a) spike raster of 10 cells; (b) membrane potential of a single cell; (c) instantaneous population firing rate; (d) distribution of firing rates across neurons; (e) power spectrum of the instantaneous population firing rate. External excitatory input is 9 kHz. Parameters: connection probability 0.1; synaptic time constants as in Fig. 7.

The A-type potassium current is an example of a membrane current that is activated below threshold and contributes to the effective membrane time constant (Connor et al. 1977) (see METHODS). When the voltage is close to threshold, an activated A-channel conductance increases the total membrane conductance, thus decreasing the effective membrane time constant τ_{m-eff} . We find that an inhibitory network of conductance-based neurons endowed with an A-type potassium current (Connor et al. 1977) can oscillate at very high frequencies (Fig. 9). With the same synaptic time constants and the same average single-cell firing rate (40 Hz) as in Fig. 7 A, the population oscillates at 220 Hz instead of 125 Hz. This dramatic increase of the population frequency compared to the network of cells without an A-type current (Fig. 7A) is explained by the fact that the effective membrane time constant is very small, $\tau_{m-eff} = 0.15$ ms in this model.

Another way to reduce τ_{m-eff} is to increase the synaptic inputs. An additional external inhibitory synaptic conductance $g_{I,ext}$ is added to the neuron model used in Fig. 7. The resulting larger effective inhibitory conductance $g_{recurrent} + g_{I,ext}$ is compensated by a larger external excitation $g_{E,ext}$, so that the average neuronal firing rate remains the same (40 Hz). Under this condition and with the same synaptic parameters, the network's rhythmic frequency becomes 180 Hz (Fig. 10A), which is significantly higher than 125 Hz in Fig. 7A. When the external excitatory and inhibitory inputs are increased in a balanced manner, the total membrane conductance $g_{tot} = g_L + g_{recurrent} + g_{I,ext} + g_{E,ext}$ increases, and $\tau_{m-eff} = 1/g_{tot}$ decreases (Fig. 10C). Concomitantly, the population frequency increases to up to 200 Hz, whereas the single-cell firing rate stays constant (Fig. 10B).

Is the change of τ_{m-eff} sufficient to account for the increase in the population frequency in these two scenarios? This question can be addressed by comparing network simulations with the theoretical prediction (Fig. 11). To predict the population frequency we first need to know the synaptic phase shift

$\phi_{I,syn}(f)$, which can be calculated from the synaptic time constants. Second, the single-cell phase shift $\phi_{I,cell}(f)$ depends on the time to peak of the spike ($\tau_{I,spike} = 0.24$ ms) and the filter time constant $\tau_{I,filter}$. The latter depends on the effective membrane time constant τ_{m-eff} and on the single cell firing rate $\tau_{I,0}$ (here $\tau_{I,0} = 40$ Hz) (Fig. 4). Using the relationship between τ_{m-eff} and $\tau_{I,filter}$ obtained from the EIF neuron model (Fig. 4D) we can predict the population rhythmic frequency of a neural network, as a function of τ_{m-eff} (Fig. 11, solid curve). The theoretical prediction agrees well with results from direct network simulations (Fig. 10B), in which the synaptic conductance was varied so that the single cell's effective membrane time constant changed from $\tau_{m-eff} = 1.5$ ms (Fig. 7) to $\tau_{m-eff} = 0.3$ ms (corresponding to large synaptic bombardment, Fig. 10). The agreement is also good for a simulated network of neurons endowed with an A-current ($\tau_{m-eff} = 0.15$ ms, population frequency of 220 Hz).

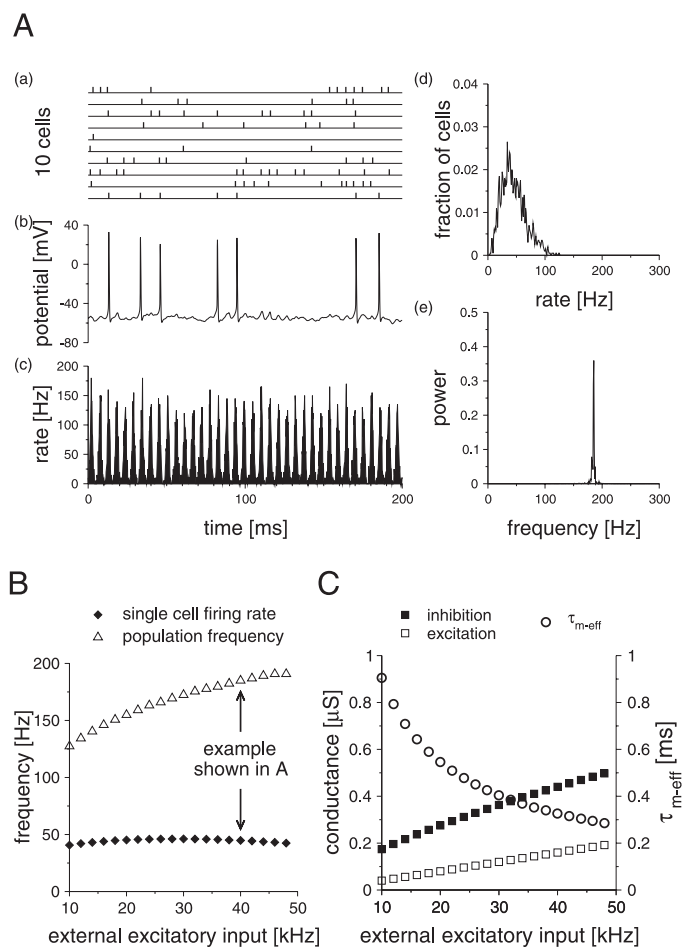


FIG. 10. A: population frequency depends on the background synaptic conductance: neurons receive strong external excitatory (40 kHz) and inhibitory (6.5 kHz) synaptic input; the network oscillates at 180 Hz, whereas single cells fire on average at 40 Hz: (a) spike raster of 10 cells; (b) membrane potential of a single cell; (c) instantaneous population firing rate; (d) distribution of single cell firing rates across the population; (e) power spectrum of the instantaneous population firing rate. B and C: each cell receives external excitatory and inhibitory Poisson inputs. Inhibitory input is adjusted so that the single-cell firing rate remains constant. B: population frequency increases with increasing input, whereas the single-cell firing rate stays constant. C: as the external inhibitory and excitatory conductances increase, the effective membrane time constant τ_{m-eff} decreases. Parameters: connection probability 0.1; synaptic time constants as in Fig. 7.

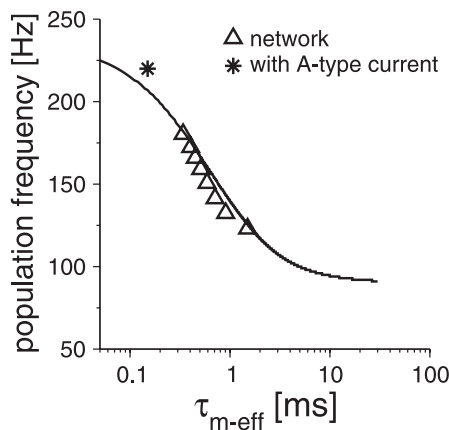


FIG. 11. Population frequency increases with decreasing effective membrane time constant. Solid curve: analytical prediction from Eq. 14 using the EIF model and the relationship between $\tau_{m\text{-eff}}$ and the gain of the r_0 - I curve $\tau_{I,filter} = (C_m \Delta_7 d r_{p,0} / dI) / r_{p,0}$ (see text and Fig. 4D); we assume the standard synaptic time constants ($\tau_{II} = 0.5$ ms, $\tau_{I,spike} = 0.24$ ms, $\tau_{Id} = 5.0$ ms) and a finite spike width ($\tau_{I,spike} = 0.24$ ms). Open triangle: simulations of networks with additional external excitatory and inhibitory synaptic input (Fig. 10B). Star: simulations of a network of interneurons with A-type potassium current (Fig. 9).

To summarize, we found that the membrane time constant of single cells strongly affects the frequency of a collective network oscillation. Because the *effective* membrane time constant $\tau_{m\text{-eff}}$ depends on the synaptic and intrinsic ion conductances, coherent oscillations as an emergent network phenomenon can have a range of frequencies that are determined and modulated by cellular and synaptic dynamics, even though single cells are dominated by noise and do not behave like oscillators.

Oscillations in a two-population network of excitatory and inhibitory neurons

We have shown that an interneuronal network can by itself generate very fast rhythms. In cortical networks, interneurons are reciprocally connected to pyramidal cells. How do the interactions with pyramidal cells affect the patterns and, in particular, the frequency of such fast oscillations? To address this question we investigate synchronous oscillations in a two-population network of inhibitory interneurons and excitatory pyramidal cells. With this type of architecture, two possible scenarios for rhythmogenesis are present: the interneuronal network and the loop between interneurons and pyramidal cells. Brunel and Wang (2003) showed that in a two-population network of LIF neurons, the oscillation frequency depends on the synaptic time constants, the relative strength between the excitatory and inhibitory synaptic currents and the connectivity among pyramidal cells. Increasing the relative strength of excitation versus inhibition typically decreases the population frequency. Including recurrent connections among pyramidal cells reduces the population frequency further.

Do these results hold for conductance-based neurons as well? Based on the single-cell simulations shown in Figs. 1–4, we expect that in a two-population network of *conductance-based* cells, the population frequency should also depend on the phase response of single interneurons and pyramidal cells to the synaptic current. We expect the population frequency to be lower than that of a network of LIF neurons. To understand

in more detail how the oscillation frequency depends on single-cell and synaptic parameters, the population frequency can be computed from both synaptic parameters and single-cell phase-shift curves, using calculations similar to those presented for a one-population network (see Fig. 12 and Appendix A). The calculation proceeds according to the following steps:

- The population firing rates of interneurons and of pyramidal cells are approximated by sinusoidal functions. These functions are characterized by the mean firing rates of interneurons ($r_{I,0}$) and pyramidal cells ($r_{P,0}$), the relative amplitude of the sinusoidal modulation (ν_I for interneurons and ν_P for pyramidal cells), and the population frequency $f = \omega/2\pi$. The firing rates of pyramidal cells and interneurons are not necessarily in phase.
- The fraction of open channels at the postsynaptic membrane follows the presynaptic firing probability with a phase delay as a result of synaptic filtering. The phase delay of the inhibitory (excitatory) synaptic currents $\phi_{I,syn}(\omega) - \pi$ [$\phi_{P,syn}(\omega)$] depends on the latency, rise, and decay time constants of the synaptic currents.
- Each neuron receives a total current that is the sum of inhibitory and excitatory synaptic currents. For the sake of simplicity, we consider here the special case when the relative strength of excitatory and inhibitory synaptic current (I_{AMPA}/I_{GABA} ratio) is the same for interneurons and pyramidal cells. The phase of the total current depends on this relative strength and on the phase difference between excitation and inhibition.
- In general, a neuron responds to the total synaptic current with a phase shift, which depends on the single-cell properties, such as firing rate and effective membrane time constant. The phase shifts of interneurons $\phi_{I,cell}(\omega)$ and pyramidal cells $\phi_{P,cell}(\omega)$ depend on the time constants $\tau_{I,spike}$, $\tau_{I,filter}$ and $\tau_{P,spike}$, $\tau_{P,filter}$ respectively, and can be determined from single cell simulations.
- Self-consistency between the presynaptic and postsynaptic firing rates, which are both the source and recipient of the recurrent synaptic input, leads to equations for the phases of excitatory and inhibitory neurons. These two equations give the frequency f of the global oscillation and the phase shift between the two populations.

The prediction is that the population frequency will be strongly affected by the effective membrane time constants of both cell types and their average firing rates, and by the relative strength of excitatory and inhibitory current.

Effect of balance between synaptic excitation and inhibition on the population frequency

We found that a wide range of frequencies can be realized in a network with the same set of synaptic time constants and the same architecture. Critical determinants of the network oscillation frequency are the level of balance between synaptic excitation and inhibition (the time-averaged I_{AMPA}/I_{GABA} ratio, which was imposed to be the same in pyramidal cells and interneurons in our simulations) and the phase shift between the excitatory and inhibitory synaptic currents. When the I_{AMPA}/I_{GABA} ratio is low, which can be achieved by very low firing rates of pyramidal cells compared to interneurons (e.g.,

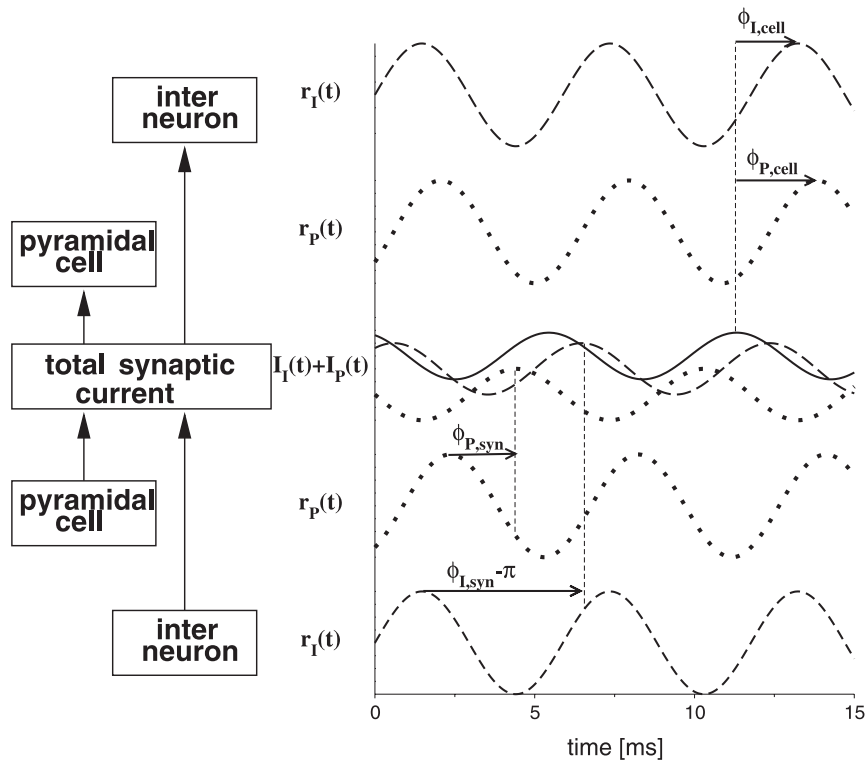


FIG. 12. Predicting the population frequency in a two-population network of interneurons and pyramidal cells: the synaptic current $I_I(t)$ of an oscillating averaged instantaneous firing rate of interneurons $r_I(t)$ is phase delayed by $\phi_{I, \text{syn}}(f) - \pi$. Synaptic current $I_P(t)$ of an oscillating averaged instantaneous firing rate of pyramidal cells $r_P(t)$ is phase delayed by $\phi_{P, \text{syn}}(f)$. Cells respond to the total synaptic current $I_I(t) + I_P(t)$ with a phase lag $\phi_{I, \text{cell}}(f)$ (interneurons) and $\phi_{P, \text{cell}}(f)$ (pyramidal cells).

interneurons fire at 35 Hz, whereas the firing rates in pyramidal cells is 1 Hz), the population frequency is mainly determined by the interneuronal network. The pyramidal cells are basically paced by the rhythmic inhibition and the population frequency is >110 Hz (Fig. 13A). On the other hand, with a high $I_{\text{AMPA}}/I_{\text{GABA}}$ ratio, the network displays synchronous gamma frequency (40 Hz) when the firing rates of pyramidal cells are high compared to interneurons (e.g., interneurons fire on average at 8 Hz and pyramidal cells on average at 3 Hz, and see Fig. 14). In that case, the oscillations are mainly maintained by the loop between interneurons and pyramidal cells.

As the $I_{\text{AMPA}}/I_{\text{GABA}}$ ratio was increased gradually starting from a low value, we observed that the population frequency can increase to up to 190 Hz (Fig. 13B), or decrease <100 Hz (data not shown). We found that a simple criterion that determines whether the population frequency increases or decreases with increasing $I_{\text{AMPA}}/I_{\text{GABA}}$ ratio is the following: if the excitatory synaptic current precedes the inhibitory synaptic current in the oscillatory cycle, then increasing $I_{\text{AMPA}}/I_{\text{GABA}}$ ratio *increases* the frequency; in the opposite situation (the excitatory current follows the inhibitory current), increasing $I_{\text{AMPA}}/I_{\text{GABA}}$ ratio *decreases* the frequency. Thus the next question is under which conditions does excitation precede or follow inhibition? These conditions are simpler to establish in the situation when the $I_{\text{AMPA}}/I_{\text{GABA}}$ ratio is the same in interneurons and in pyramidal cells and thus we restrict our discussion to this scenario. When the $I_{\text{AMPA}}/I_{\text{GABA}}$ ratio is the same in interneurons and in pyramidal cells, the total synaptic currents received by interneurons and pyramidal cells are in phase. The relative phase shift between the inhibitory and the excitatory synaptic current is (see APPENDIX B)

$$\Delta\phi_{\text{current}}(\omega) = \phi_{P, \text{syn}}(\omega) + \phi_{P, \text{cell}}(\omega) + \pi - \phi_{I, \text{syn}}(\omega) - \phi_{I, \text{cell}}(\omega) \quad (16)$$

The phase shift $\Delta\phi_{\text{current}}(\omega)$ (Eq. 16) depends on the synaptic

time constants through the synaptic phase shifts of excitation $\phi_{P, \text{syn}}(\omega)$ and inhibition $\phi_{I, \text{syn}}(\omega) - \pi$, and on the single-cell properties of pyramidal cells and interneurons through $\phi_{P, \text{cell}}(\omega)$ and $\phi_{I, \text{cell}}(\omega)$, respectively.

In Fig. 15A, we illustrate different scenarios by plotting the relative locations of the peaks of AMPA and GABA currents in an oscillatory cycle of the total synaptic current, when the $I_{\text{AMPA}}/I_{\text{GABA}}$ ratio is <1 . If in such a cycle $|\phi_{P, \text{cell}} + \phi_{P, \text{syn}}| < |\phi_{I, \text{cell}} + \phi_{I, \text{syn}}|$ (respectively $|\phi_{P, \text{cell}} + \phi_{P, \text{syn}}| > |\phi_{I, \text{cell}} + \phi_{I, \text{syn}}|$) I_{AMPA} follows (respectively precedes) I_{GABA} . As a first example, consider the case in which $\phi_{P, \text{cell}}(\omega) = \phi_{I, \text{cell}}(\omega)$, and excitatory time constants are shorter than inhibitory time constants, $|\phi_{P, \text{syn}}(\omega)| < |\phi_{I, \text{syn}}(\omega)|$ [Fig. 15A(i)]. Then $\Delta\phi_{\text{current}}(\omega) > 180^\circ$, excitation follows inhibition, and therefore an increase in excitation strength will decrease the oscillation frequency. This is the scenario that was considered in Brunel and Wang (2003). On the other hand, if the single-cell phase shift of pyramidal cells is sufficiently larger than that of interneurons, due to a larger $\tau_{m\text{-eff}}$ and/or $\tau_{P, \text{spike}}$, then $\Delta\phi_{\text{current}}(\omega)$ can become $<180^\circ$, and excitation now precedes inhibition [Fig. 15A(ii)]. Thus, somewhat counterintuitively, a larger neuronal phase shift of pyramidal cells would favor the regime where an increased $I_{\text{AMPA}}/I_{\text{GABA}}$ ratio accelerates the network oscillation.

Another scenario that leads to excitation preceding inhibition is a scenario in which the latency of AMPA currents is larger than the latency of GABA currents. If $\tau_{\text{AMPA-latency}} > \tau_{\text{GABA-latency}}$ but the sum of all synaptic time constants is shorter for AMPA than for GABA, then we observe a frequency-dependent effect: for low frequencies $|\phi_{I, \text{syn}}(\omega)| > |\phi_{P, \text{syn}}(\omega)|$, and consequently inhibition precedes excitation [Fig. 15A(iv)], whereas for sufficiently high frequencies the latency dominates the synaptic phase shift, $|\phi_{I, \text{syn}}(\omega)| < |\phi_{P, \text{syn}}(\omega)|$, and consequently excitation precedes inhibition [Fig. 15A(iii)]. Thus depending on the

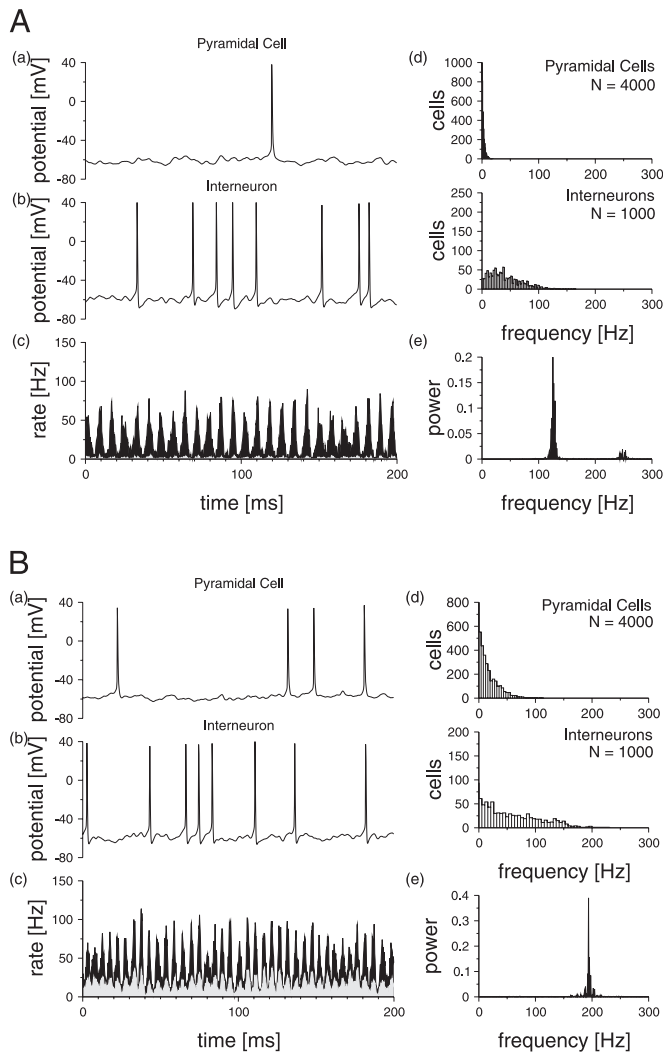


FIG. 13. A two-population network can oscillate at different frequencies depending on the balance of excitatory and inhibitory synaptic currents. In both cases are shown the membrane voltage of a single pyramidal cell (a) and interneuron (b); the instantaneous population firing rate of pyramidal cells (gray) and interneurons (black) (c); the distribution of the single cell firing rates across the population (d); and the power spectrum of the instantaneous population firing rate of pyramidal cells (e). *A*: high-frequency oscillations (125 Hz). I_{AMPA}/I_{GABA} ratio is essentially zero and the population frequency is mainly determined by the interneuronal network. Average single-cell firing rates: pyramidal cells 1 Hz, interneurons 35 Hz. External input to pyramidal cells 3 kHz, to interneurons 4.5 kHz. *B*: high-frequency oscillations (190 Hz). When the I_{AMPA}/I_{GABA} ratio is not zero but low, the population frequency is determined by the interneuronal network and the interneuron–pyramidal cell loop. Average single-cell firing rate: pyramidal cells 15 Hz and interneurons 40 Hz. External input to pyramidal cells 5.06 kHz and to interneurons 5.6 kHz. Synaptic time constants: GABA $\tau_{il} = 0.5$ ms, $\tau_{ir} = 0.5$ ms, $\tau_{id} = 5.0$ ms; AMPA $\tau_{pl} = 1.5$ ms, $\tau_{pr} = 0.5$ ms, $\tau_{pd} = 2.0$ ms; connection probability 0.1.

latency of AMPA currents, increasing the I_{AMPA}/I_{GABA} ratio can lead to a monotonic decrease of the oscillation frequency (if latency is sufficiently short), or an increase followed by a decrease of the oscillation frequency (if latency is sufficiently large). Figure 15*B* illustrates the situation with a short latency of AMPA currents, $\tau_{AMPA-latency} = 0.5$ ms. The excitatory current follows the inhibitory current for all values of the I_{AMPA}/I_{GABA} ratio. The frequency of the oscillations is 130 Hz for $I_{AMPA}/I_{GABA} = 0$ and decreases to gamma oscillations (40 Hz) at $I_{AMPA}/I_{GABA} = 1$. In

the second case, the excitatory current *precedes* the inhibitory current and the population frequency *increases* with increasing I_{AMPA}/I_{GABA} ratio for small I_{AMPA}/I_{GABA} ratios. An increase in excitation leads to a larger phase advance of the total current compared to inhibition, which shortens the oscillatory cycle and leads to a higher population frequency. However, the range of the

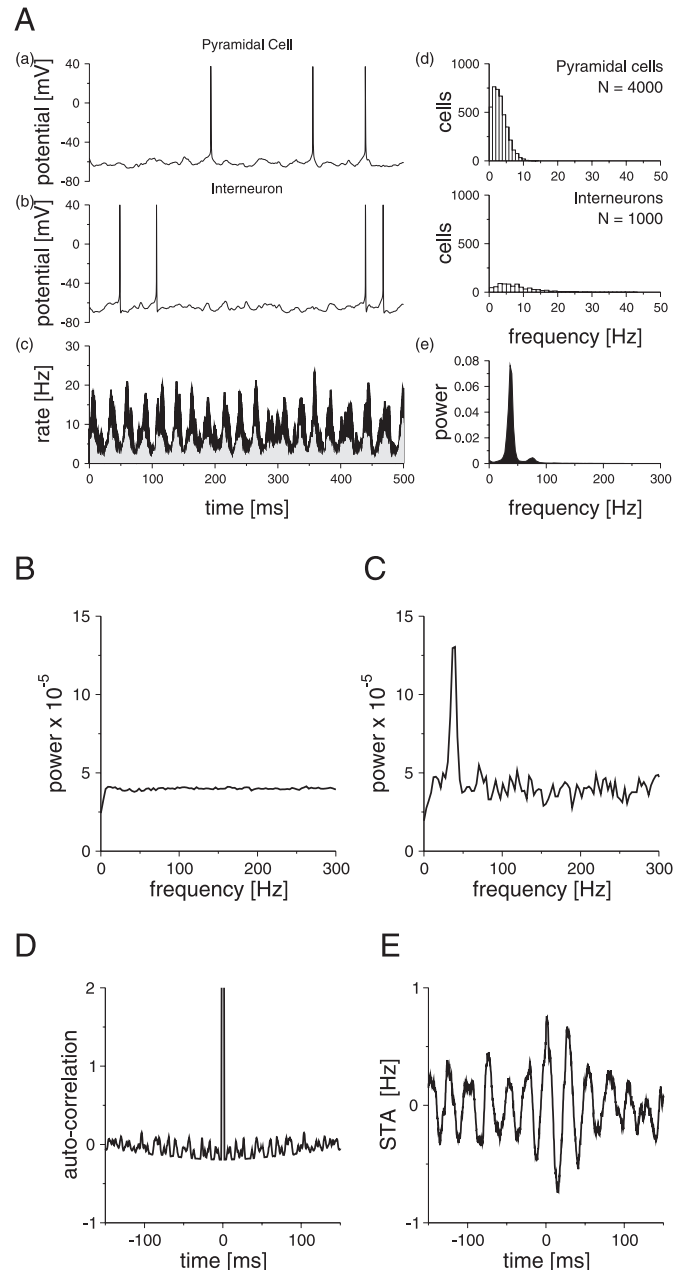


FIG. 14. A two-population network oscillates at gamma frequency (40 Hz). *A*: membrane voltage of a single pyramidal cell (a) and interneuron (b), the instantaneous population firing rate of pyramidal cells (gray) and interneurons (black) (c), the distribution of the single cell firing rates across the population (d), and the power spectrum of the instantaneous population firing rate of pyramidal cells (e). Average single-cell firing rates: pyramidal cells 3 Hz, interneurons 8 Hz. External input to pyramidal cells 0.82 kHz, to interneurons 0.4 kHz. *B*: oscillations are not detectable in the power spectrum of single-cell spike trains. *C*: power spectrum of multiunit activity averaged over 50 spike trains shows a clear peak at 40 Hz. *D*: autocorrelation of a single spike train (averaged over 50 cells) does not show a clear oscillatory pattern. *E*: STA of the population rate shows oscillations at gamma frequency. Spike-triggered population rate is averaged over the spikes of one neuron (52 spikes). Length of spike train: 10 s. Synaptic parameters as in Fig. 13.

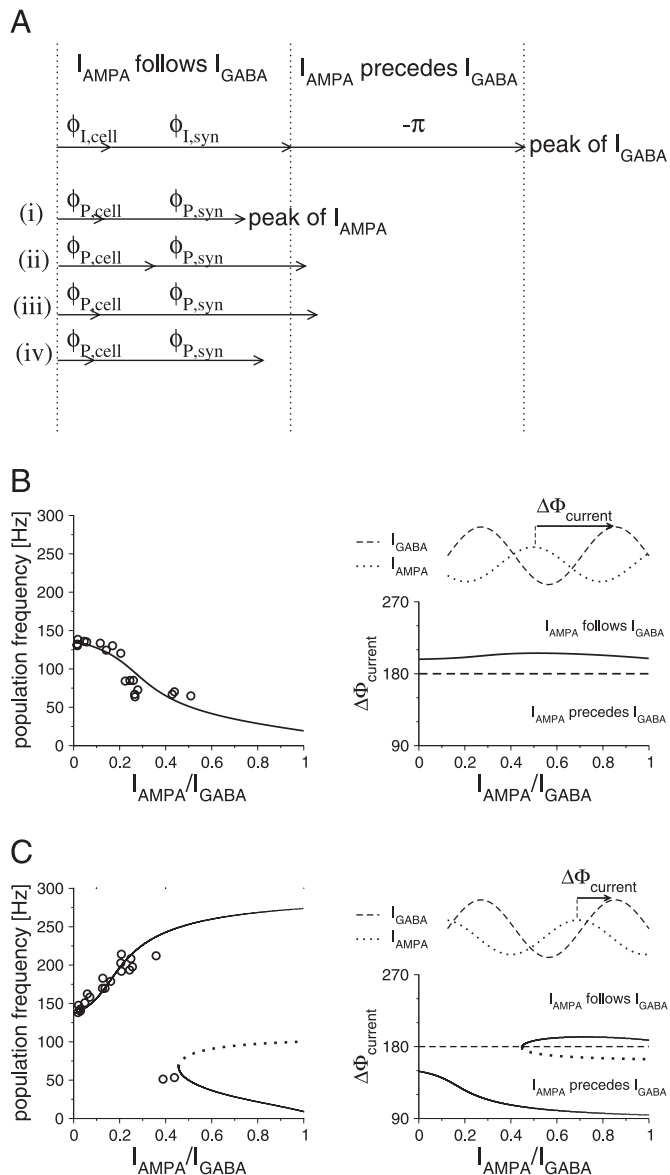


FIG. 15. Population frequency depends on the balance (I_{AMPA}/I_{GABA}) and on the relative phase shift between the excitatory and inhibitory synaptic currents $\Delta\Phi_{current} = \phi_{P,syn}(f) + \phi_{P,cell}(f) - \phi_{I,syn}(f) - \phi_{I,cell}(f) + \pi$. **A**: illustration of different scenarios that can lead to excitatory current I_{AMPA} following (i) and (iv) or preceding (ii) and (iii) inhibitory current I_{GABA} , respectively (see text). **B**, left: population frequency decreases with increasing recurrent excitation when excitation follows inhibition. Right: phase shift $\Delta\Phi_{current}$ is $>180^\circ$ for all values of I_{AMPA}/I_{GABA} . Excitatory synaptic current follows the inhibitory synaptic current, as illustrated in the top trace ($\tau_{AMPA-latency} = 0.5$ ms; all other synaptic parameters as in Fig. 13). **C**, left: population frequency increases with increasing recurrent excitation when excitation precedes inhibition. Right: for small values of I_{AMPA}/I_{GABA} the excitatory synaptic current precedes the inhibitory synaptic current, as illustrated in the top trace. There is a critical I_{AMPA}/I_{GABA} ratio, above which a second stable solution becomes possible and the trend is reversed: the oscillation frequency shows a discrete drop from ripple frequency to gamma frequency range (solid line: stable solution; dotted line: unstable solution). ($\tau_{AMPA-latency} = 1.5$ ms; all other synaptic parameters as in Fig. 13). Solid/dotted curves: analytical prediction; open circle: network simulations.

I_{AMPA}/I_{GABA} ratio within which the excitatory synaptic current precedes the inhibitory synaptic current is limited. Starting with a network in which only interneurons are active, an increase in excitation leads to an increase in the population frequency, but

only until the oscillation cycle is shortened such that the excitatory current turns from preceding into following inhibition. The excitatory current precedes the inhibitory current [$0 < \Delta\phi_{current}(\omega) < 180$] for a range of small I_{AMPA}/I_{GABA} but follows the inhibitory current [$180 < \Delta\phi_{current}(\omega) < 360$] for large I_{AMPA}/I_{GABA} (Fig. 15C). This leads to two well-separated frequency regimes: population frequencies >120 Hz for small I_{AMPA}/I_{GABA} ratios and <80 Hz for larger I_{AMPA}/I_{GABA} ratios for the parameters of Fig. 15C. When the excitatory current peaks before the inhibitory current (with a synaptic latency of excitation $\tau_{AMPA-latency} = 1.5$ ms), the population frequency can reach the 200-Hz range, with single cells remaining at much lower rates (Fig. 13B). We note again that I_{AMPA} preceding I_{GABA} does not necessarily require longer synaptic latency for excitation than for inhibition; slower intrinsic time constants in excitatory neurons would also be sufficient to give rise to this phenomenon.

The phase shift between the firing rates of interneurons and pyramidal cells depends only on single-cell characteristics

$$\Delta\phi_{rate}(\omega) = \phi_{P,cell}(\omega) - \phi_{I,cell}(\omega) \quad (17)$$

when the I_{AMPA}/I_{GABA} ratio is the same in interneurons and pyramidal cells (APPENDIX B). When $\Delta\phi_{rate} > 0$ interneurons follow pyramidal cells. For LIF neurons $\Delta\phi_{rate} = 0$, because interneurons and pyramidal cells respond to oscillating synaptic current with negligible phase lag and, as a consequence, both populations oscillate in phase. On the other hand, conductance-based neurons generally respond to oscillating synaptic currents with a phase lag that is larger for pyramidal cells than that for interneurons. When the I_{AMPA}/I_{GABA} ratio is the same in pyramidal cells and interneurons, pyramidal cells tend to follow interneurons. However, when recurrent connections among pyramidal cells are absent, or more generally when the ratio of excitation to inhibition is weaker in pyramidal cells than in interneurons, pyramidal cells tend to precede interneurons (Brunel and Wang 2003).

DISCUSSION

During certain behavioral states, neocortex and hippocampus display fast (40–200 Hz) oscillations that are detected in the local field potential, but not easily in spike trains of individual neurons that are typically very irregular (Engel et al. 1992; Fries et al. 2001a,b; Logothetis et al. 2001). This is at odds with most theoretical studies of network synchronization, in which neurons are coupled oscillators (Borgers and Kopell 2003; Ermentrout and Rinzel 1984; Gerstner et al. 1996; Hansel et al. 1995; Kopell and LeMasson 1994; Marder 1998; Nomura et al. 2003; Traub et al. 1996; van Vreeswijk et al. 1994; Wang and Buzsáki 1996). On the other hand, rhythmic phenomena that mimic the phenomenology of fast oscillations occur in networks in which single neurons are subject to large amounts of noise, which can be attributed either to external inputs or to intrinsic network dynamics in networks with sparse and random connectivity (Brunel 2000; Brunel and Hakim 1999; Brunel and Wang 2003). The present study represents a further step along this line of research, and extends the theoretical framework to networks of Hodgkin–Huxley-type conductance-based models. We showed that the frequency of network oscillations is determined by the interplay between synaptic kinetics and the single cell's spiking properties. We extended a theoretical framework for predicting the population

frequency, on the basis of quantitative synaptic kinetic properties and the response properties of single cells.

Collective network rhythmic frequency depends on single-cell spiking properties

In sharp contrast to the LIF model, the firing response of a single conductance-based model neuron to a noisy sinusoidal input strongly depends on the stimulus frequency (see also Fourcaud-Trocmé et al. 2003). This cellular response property has a major impact on the frequency of synchronous network oscillations. In interneuronal networks, with the same network connectivity, same synaptic time constants, and same average firing rates of single neurons, varying the single-cell properties alone can change the network rhythmic frequency by a significant amount (e.g., from 100 to 200 Hz). The present study shows that, when single neurons fire irregularly and fast coherent oscillation is an emergent network phenomenon, synchronization properties (in particular the frequency) depend critically on the membrane dynamics that control the upstroke of action potentials. This is explicitly demonstrated by the exponential integrate-and-fire model that, with just one non-linear voltage dependence, is shown to adequately account for the single cell's impact on the network oscillation frequency.

Moreover, we show that the membrane time constant of single cells greatly affects the frequency of network oscillations. An increased total membrane conductance, described either to spontaneous synaptic activity (Borg-Graham et al. 1998; Chance et al. 2002; Destexhe and Paré 1999; Häusser et al. 2001) or to intrinsic ion channels (Connor et al. 1977; Softky 1994) leads to a smaller effective membrane time constant, which favors a higher population rhythmic frequency. Thus the general conclusions of Brunel and Wang (2003) that an interneuronal network of inhibitory cells can give rise to >100 Hz coherent oscillations with irregular neural discharges still holds. However, the effective membrane time constant needs to be <0.5 ms in the models we considered here to achieve a 200-Hz oscillation. It is not known whether such a short effective membrane time constant is realized in real neurons *in vivo*. Another parameter that strongly influences the phase lag of single cells at high frequency is the sharpness of spike initiation, as measured by the parameter Δ_T of the EIF model (Fourcaud-Trocmé et al. 2003). Thus if real neurons have significantly sharper spike initiation than the Hodgkin-Huxley-type models considered here, 200-Hz oscillations could be sustained with larger effective membrane time constants.

To predict the frequency of weakly synchronous rhythms in a noise-dominated network, it is necessary to quantitatively characterize the responsiveness of single cells to a noisy sinusoidal input (see also Fuhrmann et al. 2002). We showed that a Hodgkin-Huxley-like conductance-based neuron has a smaller response amplitude and larger phase lag with increasingly higher input frequency. This modulation is independent of the synaptic time constant, in contrast to the LIF model for which the frequency dependency becomes negligible when the synaptic time constant becomes comparable to or larger than the neuronal membrane time constant (Brunel et al. 2001). The phase lag can be approximately described by the sum of a linear filter, related to the membrane dynamics for the upstroke leading to a spike threshold; and a constant phase shift related

to the spike time to peak. The time constant for the linear filter is shorter with smaller effective membrane time constant and higher single-cell firing rate. This leads to a smaller phase lag of single cells, which implies faster population frequency in the network. Note that our approach with a filter is only a phenomenological description. Other single-cell conductance-based models display phase advance at low frequencies arising from negative feedback mechanisms (Fuhrmann et al. 2002; Richardson et al. 2003; Shriki et al. 2003). However, these phase-advance phenomena are generally observed at much lower frequencies than the network frequencies investigated in this paper, and they should not interfere with the mechanisms giving rise to the fast network oscillation, although they could modulate such an oscillation slowly.

Fast oscillations in two-population network of pyramidal cells and interneurons

In this paper, we examined rhythmogenesis both in a one-population network of inhibitory interneurons and in a two-population network of interneurons and pyramidal cells. The oscillation frequency in a two-population network of conductance-based neurons depends strongly on the current balance ($I_{\text{AMPA}}/I_{\text{GABA}}$ ratio) and time constants of excitatory and inhibitory synaptic interactions, as has been shown in the network of LIF neurons (Brunel and Wang 2003). It has been shown that strong recurrent excitation typically reduces the oscillation frequency in a two-population network of LIF neurons, compared to the purely interneuronal network (Brunel and Wang 2003). We observed that intrinsic and/or synaptic dynamics of excitatory neurons, which are slower than those of inhibitory interneurons, can lead to *faster* rhythmic frequencies in the two-population network, compared to the purely interneuronal network. Intuitively, this happens when the combined (synaptic and cellular) phase lag for excitation exceeds that for inhibition by >180°, so that excitation appears to be in advance of inhibition. Under this condition, 200-Hz oscillations can be realized even with reasonable effective membrane time constants (≈ 1.2 ms), unlike the purely interneuronal network. Moreover, because the population frequency is larger with higher single-cell firing rates, it is easier to realize 200-Hz network rhythms with increased neural activity. This is in consonance with the experimental observation that single-cell firing rates increase significantly during 200-Hz sharp-wave ripples compared to non-sharp-wave episodes (Csicsvari et al. 1999b). In the scenario in which recurrent excitation increases the population frequency at low $I_{\text{AMPA}}/I_{\text{GABA}}$ ratios, one can distinguish two well-separated frequency bands: a high-frequency band (120–250 Hz) at low $I_{\text{AMPA}}/I_{\text{GABA}}$ ratios; and the gamma frequency band (40–80 Hz) at larger $I_{\text{AMPA}}/I_{\text{GABA}}$ ratios.

Our analysis of rhythmogenesis in a recurrent network of noisy neurons requires knowledge of synaptic kinetics and strength, as well as of how a single cell responds to noisy sinusoidal inputs. Thus it is crucial to examine experimentally how cortical neurons (both pyramidal cells and interneurons) respond to a weak oscillatory input in the presence of a large amount of noise, and especially how the response amplitude and phase depend on the input frequency. The present study also highlights the importance of measuring the ratio of the mean excitatory and inhibitory currents (Anderson et al. 2000;

Borg-Graham et al. 1996; Compte et al. 2003; Shu et al. 2003) and, in particular, examining whether this ratio is roughly the same in interneurons and pyramidal cells.

If the $I_{\text{AMPA}}/I_{\text{GABA}}$ ratio is the same in two cell types, the phase lag of firing rates between the two populations is solely determined by the single cell's properties. Recently, it was found that pyramidal cells precede fast-spiking interneurons by 90° during fast oscillations (Csicsvari et al. 1999b; Klausberger et al. 2003). In a network in which the excitation–inhibition balance is the same in two cell types, such an experimental finding could be accommodated only if interneurons have a larger cellular phase shift than that of pyramidal cells. On the other hand, such a phase shift between firing rates can be accounted for in a network in which the excitation–inhibition balance is lower in pyramidal cells than that in interneurons (Brunel and Wang 2003). In this scenario, the high network frequency could be compatible only with very small single-cell filter time constants, which could be obtained by a massive increase of input conductance, and/or a very sharp spike initiation.

To conclude, we have developed a theoretical framework for predicting the rhythmic frequency and relative phase relationship between cell populations for a noisy neural network, in terms of cellular and synaptic biophysical properties. This work helps to reconcile the apparent dichotomy between oscillatory local field potentials and almost Poisson-like stochastic spike discharges of single neurons, a characteristic of fast coherent oscillations observed in the neocortex of awake behaving animals (Averbeck and Lee 2004; Baker et al. 2001; Fries et al. 2001b).

APPENDIX A

Oscillation frequency of a two-population network

The presynaptic firing rates of interneurons and pyramidal cells are

$$\begin{aligned} r_P(t) &= r_{P,0}[1 + v_P e^{i\omega t}] \\ r_I(t) &= r_{I,0}[1 + v_I e^{i\omega t}] \end{aligned} \quad (\text{A1})$$

where $r_{P,0}$ and $r_{I,0}$ are the mean rates of interneurons and pyramidal cells, respectively, and v_P and v_I are relative deviations from the mean. The fraction of open channels follows the firing rate with a phase lag as a result of the synaptic filtering

$$\begin{aligned} s_{\text{AMPA}}(t) &= s_{\text{AMPA},0}\{1 + v_P S_P(\omega) e^{[i\omega t + i\phi_{P,\text{syn}}(\omega)]}\} + \text{noise} \\ s_{\text{GABA}}(t) &= s_{\text{GABA},0}\{1 + v_I S_I(\omega) e^{[i\omega t + i\phi_{I,\text{syn}}(\omega)]}\} + \text{noise} \end{aligned} \quad (\text{A2})$$

where the attenuation in the amplitude of the oscillation induced by synaptic filtering

$$\begin{aligned} S_P(\omega) &= \frac{1}{\sqrt{(1 + \omega^2 \tau_{Pd}^2)(1 + \omega^2 \tau_{Pr}^2)}} \\ S_I(\omega) &= \frac{1}{\sqrt{(1 + \omega^2 \tau_{Id}^2)(1 + \omega^2 \tau_{Ir}^2)}} \end{aligned} \quad (\text{A3})$$

and the phase introduced by synaptic filtering

$$\begin{aligned} \phi_{P,\text{syn}}(\omega) &= -\omega\tau_{PI} - \text{atan}(\omega\tau_{Pr}) - \text{atan}(\omega\tau_{Pd}) \\ \phi_{I,\text{syn}}(\omega) &= -\omega\tau_{II} - \text{atan}(\omega\tau_{Ir}) - \text{atan}(\omega\tau_{Id}) \end{aligned} \quad (\text{A4})$$

depend on the synaptic time constants: latency τ_{PI} , rise τ_{Pr} , and decay τ_{Pd} time for excitation; and latency τ_{II} , rise τ_{Ir} , and decay τ_{Id} time for

inhibition. Neglecting fluctuations in the driving force, the synaptic current can be written as

$$\begin{aligned} I_{\text{AMPA}}(t) &= I_{\text{AMPA},0}\{1 + v_P S_P(\omega) e^{[i\omega t + i\phi_{P,\text{syn}}(\omega)]}\} + \text{noise} \\ I_{\text{GABA}}(t) &= I_{\text{GABA},0}\{1 + v_I S_I(\omega) e^{[i\omega t + i\phi_{I,\text{syn}}(\omega) - \pi]}\} + \text{noise} \end{aligned} \quad (\text{A5})$$

The factor $-\pi$ comes from the fact that $I_{\text{GABA}}(t)$ is an inhibitory current and is therefore phase-reversed compared to the fraction of open channels $s_{\text{GABA}}(t)$. The total synaptic current for interneurons and pyramidal cells is a superposition of excitatory and inhibitory current

$$\begin{aligned} I_P(t) &= I_{\text{AMPA} \rightarrow P} + I_{\text{GABA} \rightarrow P} + I_{P,\text{ext}} + \text{noise} \\ &= I_{\text{tot} \rightarrow P,0}\{1 + I_{PP} v_P S_P(\omega) e^{[i\omega t + i\phi_{P,\text{syn}}(\omega)]} + I_{IP} v_I S_I(\omega) e^{[i\omega t + i\phi_{I,\text{syn}}(\omega) - \pi]}\} + I_{\text{noise}} \\ I_I(t) &= I_{\text{AMPA} \rightarrow I} + I_{\text{GABA} \rightarrow I} + I_{I,\text{ext}} + \text{noise} \\ &= I_{\text{tot} \rightarrow I,0}\{1 + I_{PI} v_P S_P(\omega) e^{[i\omega t + i\phi_{P,\text{syn}}(\omega)]} + I_{II} v_I S_I(\omega) e^{[i\omega t + i\phi_{I,\text{syn}}(\omega) - \pi]}\} + I_{\text{noise}} \end{aligned} \quad (\text{A6})$$

where

$$I_{PP} = \frac{I_{\text{AMPA} \rightarrow P,0}}{I_{\text{tot} \rightarrow P,0}} \quad I_{IP} = \frac{I_{\text{GABA} \rightarrow P,0}}{I_{\text{tot} \rightarrow P,0}} \quad I_{PI} = \frac{I_{\text{AMPA} \rightarrow I,0}}{I_{\text{tot} \rightarrow I,0}} \quad I_{II} = \frac{I_{\text{GABA} \rightarrow I,0}}{I_{\text{tot} \rightarrow I,0}} \quad (\text{A7})$$

The postsynaptic firing rate follows the synaptic current, but with an additional phase shift

$$\begin{aligned} r_P(t) &= r_{P,0}\{1 + \beta_P A_P(\omega) e^{[i\omega t + i\phi_{P,\text{cell}}(\omega)]} \\ &\quad \times [I_{PP} v_P S_P(\omega) e^{i\phi_{P,\text{syn}}(\omega)} + I_{IP} v_I S_I(\omega) e^{i\phi_{I,\text{syn}}(\omega) - i\pi}]\} \\ r_I(t) &= r_{I,0}\{1 + \beta_I A_I(\omega) e^{[i\omega t + i\phi_{I,\text{cell}}(\omega)]} \\ &\quad \times [I_{PI} v_P S_P(\omega) e^{i\phi_{P,\text{syn}}(\omega)} + I_{II} v_I S_I(\omega) e^{i\phi_{I,\text{syn}}(\omega) - i\pi}]\} \end{aligned} \quad (\text{A8})$$

where $\phi_{P,\text{cell}}(\omega)$ and $\phi_{I,\text{cell}}(\omega)$ are the phase shifts attributed to intrinsic cell properties. $A_P(\omega)$ and $A_I(\omega)$ are normalized oscillation amplitudes of the firing rates, and β_P and β_I are the gains of the r_0 – I curves at the frequency r_0 .

To find the self-consistent solution we equate the pre- and postsynaptic firing rates (Eqs. A1 and A8, respectively) of pyramidal cells and of interneurons

$$v_P = e^{i\phi_{P,\text{cell}}(\omega)} [v_P X_{PP}(\omega) e^{i\phi_{P,\text{syn}}(\omega)} + v_I X_{IP}(\omega) e^{i\phi_{I,\text{syn}}(\omega) - i\pi}] \quad (\text{A9})$$

$$v_I = e^{i\phi_{I,\text{cell}}(\omega)} [v_P X_{PI}(\omega) e^{i\phi_{P,\text{syn}}(\omega)} + v_I X_{II}(\omega) e^{i\phi_{I,\text{syn}}(\omega) - i\pi}] \quad (\text{A10})$$

which leads to

$$\begin{aligned} 1 &= X_{II}(\omega) e^{i\phi_{I,\text{cell}}(\omega) - i\pi} + X_{PP}(\omega) e^{i\phi_{P,\text{cell}}(\omega)} \\ &\quad + (X_{IP}(\omega) X_{PI}(\omega) - X_{PP}(\omega) X_{II}(\omega)) e^{i\phi_{P,\text{cell}}(\omega) + i\phi_{I,\text{cell}}(\omega) - i\pi} \end{aligned} \quad (\text{A11})$$

where the amplitude $X_{\gamma\delta}(\omega)$ and phase $\tilde{\phi}_\gamma(\omega)$ are given as

$$X_{\gamma\delta}(\omega) = \beta_\delta A_\delta(\omega) I_{\gamma\delta} S_\gamma(\omega) \quad \text{and} \quad \tilde{\phi}_\gamma(\omega) = \phi_{\gamma,\text{syn}}(\omega) + \phi_{\gamma,\text{cell}}(\omega) \quad (\text{A12})$$

with $\gamma, \delta = \{P, I\}$. In general the ratio of excitation and inhibition is not the same for interneurons and pyramidal cells but might differ by a factor α

$$\frac{I_{PP}}{I_{IP}} = \alpha \frac{I_{PI}}{I_{II}} \quad (\text{A13})$$

Note that this is equivalent to $X_{PP}(\omega)/X_{IP}(\omega) = \alpha X_{PI}(\omega)/X_{II}(\omega)$. We can now write down the condition for the phase that determines the population frequency

$$\frac{I_{PP}}{I_{II}} = \frac{\beta_p A_p(\omega) S_p(\omega) \sin \tilde{\phi}_p(\omega)}{\beta_p A_p(\omega) S_p(\omega) \sin \tilde{\phi}_p(\omega)} + (1 - \alpha) A_p(\omega) \beta_p S_p(\omega) \frac{I_{PI} I_{PP} \sin [\tilde{\phi}_p(\omega) + \tilde{\phi}_I(\omega)]}{I_{II} \sin \tilde{\phi}_p(\omega)} \quad (A14)$$

When the ratio of excitation and inhibition is the same for interneurons and pyramidal cells ($\alpha = 1$), the population frequency is simply given by

$$\frac{I_{PP}}{I_{II}} = \frac{\beta_p A_p(\omega) S_p(\omega) \sin \tilde{\phi}_p(\omega)}{\beta_p A_p(\omega) S_p(\omega) \sin \tilde{\phi}_p(\omega)} \quad (A15)$$

In this case, the population frequency depends only on the ratio of excitatory and inhibitory current (I_{PP}/I_{II}) and the synaptic and single-cell properties of interneurons and pyramidal cells.

APPENDIX B

The relative phase between excitatory and inhibitory neurons

The postsynaptic firing rate (Eq. A8) can be written in the form

$$r_p(t) = r_{p,0} [1 + v_p(\omega) e^{i(\omega t + i\Delta\phi_{rate}(\omega))}]$$

$$r_I(t) = r_{I,0} [1 + v_I(\omega) e^{i\omega t}] \quad (B1)$$

which allows a direct comparison of the two firing rate probabilities. The phase difference $\Delta\phi_{rate}(\omega)$ and the amplitude can be calculated from Eqs. A9–A11. The amplitude is

$$v_p = v_I \frac{X_{IP}(\omega)}{X_{II}(\omega)} \times \frac{1}{\sqrt{1 + (1 - \alpha)^2 \left[\frac{X_{IP}(\omega) X_{PI}(\omega)}{X_{II}(\omega)} \right]^2 + 2(1 - \alpha) \frac{X_{IP}(\omega) X_{PI}(\omega)}{X_{II}(\omega)} \cos [\tilde{\phi}_p(\omega)]}} \quad (B2)$$

and the phase is given by

$$\Delta\phi_{rate}(\omega) = \phi_{p,cell}(\omega) - \phi_{I,cell}(\omega) - \text{atan} \left[\frac{(1 - \alpha) \frac{X_{IP}(\omega) X_{PI}(\omega)}{X_{II}(\omega)} \sin \tilde{\phi}_p(\omega)}{1 + (1 - \alpha) \frac{X_{IP}(\omega) X_{PI}(\omega)}{X_{II}(\omega)} \cos \tilde{\phi}_p(\omega)} \right] \quad (B3)$$

The phase shift between excitatory and inhibitory currents can be derived from

$$I_{AMPA}(t) = I_{AMPA,0} \{1 + v_p S_p(\omega) e^{[i\omega t + i\Delta\phi_{rate}(\omega) + i\phi_{p,syn}(\omega)]}\} + \text{noise}$$

$$I_{GABA}(t) = I_{GABA,0} \{1 + v_I S_I(\omega) e^{[i\omega t + i\phi_{I,syn}(\omega) - i\pi]}\} + \text{noise} \quad (B4)$$

and is then

$$\Delta\phi_{current} = \Delta\phi_{rate}(\omega) + \phi_{p,syn}(\omega) - \phi_{I,syn}(\omega) + \pi$$

$$= \phi_{p,cell}(\omega) + \phi_{p,syn}(\omega) - \phi_{I,cell}(\omega) - \phi_{I,syn}(\omega) + \pi - \text{atan} \left[\frac{(1 - \alpha) \frac{X_{IP}(\omega) X_{PI}(\omega)}{X_{II}(\omega)} \sin \tilde{\phi}_p(\omega)}{1 + (1 - \alpha) \frac{X_{IP}(\omega) X_{PI}(\omega)}{X_{II}(\omega)} \cos \tilde{\phi}_p(\omega)} \right] \quad (B5)$$

In the balanced case, when $\alpha = 1$, the phase differences reduce to

$$\Delta\phi_{rate} = \phi_{p,cell}(\omega) - \phi_{I,cell}(\omega) \quad (B6)$$

$$\Delta\phi_{current} = \phi_{p,cell}(\omega) + \phi_{p,syn}(\omega) - \phi_{I,cell}(\omega) - \phi_{I,syn}(\omega) + \pi \quad (B7)$$

GRANTS

This work was supported in part by National Institute of Mental Health Grant MH-62349 and the Swartz Foundation to C. Geisler and X.-J. Wang.

REFERENCES

- Anderson JS, Carandini M, and Ferster D.** Orientation tuning of input conductance, excitation, and inhibition in cat primary visual cortex. *J Neurophysiol* 84: 909–926, 2000.
- Angulo MC, Rossier J, and Audinat E.** Postsynaptic glutamate receptors and integrative properties of fast-spiking interneurons in the rat neocortex. *J Neurophysiol* 82: 1295–1302, 1999.
- Averbeck BB and Lee D.** Coding and transmission of information by neural ensembles. *Trends Neurosci* 27: 225–230, 2004.
- Azouz R and Gray CM.** Dynamic spike threshold reveals a mechanism for synaptic coincidence detection in cortical neurons in vivo. *Proc Natl Acad Sci USA* 97: 8110–8115, 2000.
- Baker SN, Spinks R, Jackson A, and Lemon RN.** Synchronization in monkey motor cortex during a precision grip task. I. Task-dependent modulation in single-unit synchrony. *J Neurophysiol* 85: 869–885, 2001.
- Bartos M, Vida I, Frotscher M, Geiger JRP, and Jonas P.** Rapid signaling at inhibitory synapses in a dentate gyrus interneuron network. *J Neurosci* 21: 2687–2698, 2001.
- Bartos M, Vida I, Frotscher M, Meyer A, Monyer H, Geiger JRP, and Jonas P.** Fast synaptic inhibition promotes synchronized gamma oscillations in hippocampal interneuron networks. *Proc Natl Acad Sci USA* 99: 13222–13227, 2002.
- Borg-Graham L, Monier C, and Frégnac Y.** Voltage-clamp measurement of visually-evoked conductances with whole-cell patch recordings in primary visual cortex. *J Physiol (Paris)* 90: 185–188, 1996.
- Borg-Graham LJ, Monier C, and Frégnac Y.** Visual input evokes transient and strong shunting inhibition in visual cortical neurons. *Nat Neurosci* 393: 369–373, 1998.
- Borgers C and Kopell N.** Synchronization in networks of excitatory and inhibitory neurons with sparse, random connectivity. *Neural Comput* 15: 509–538, 2003.
- Brunel N.** Dynamics of sparsely connected networks of excitatory and inhibitory spiking neurons. *J Comput Neurosci* 8: 183–208, 2000.
- Brunel N, Chance F, Fourcaud N, and Abbott L.** Effects of synaptic noise and filtering on the frequency response of spiking neurons. *Phys Rev Lett* 86: 2186–2189, 2001.
- Brunel N and Hakim V.** Fast global oscillations in networks of integrate-and-fire neurons with low firing rates. *Neural Comput* 11: 1621–1671, 1999.
- Brunel N and Wang X.-J.** What determines the frequency of fast network oscillations with irregular neural discharges? I. Synaptic dynamics and excitation–inhibition balance. *J Neurophysiol* 90: 415–430, 2003.
- Buhl EH, Han ZS, Lorinczi Z, Stezhka VV, Karnup SV, and Somogyi P.** Physiological properties of anatomically identified axo-axonic cells in the rat hippocampus. *J Neurophysiol* 71: 1289–1307, 1994.
- Buhl EH, Tamas G, and Fisahn A.** Cholinergic activation and tonic excitation induce persistent gamma oscillations in mouse somatosensory cortex in vitro. *J Physiol* 513: 117–126, 1998.
- Buhl EH, Tamas G, Szilagyí T, Stricker C, Paulsen O, and Somogyi P.** Effect, number and location of synapses made by single pyramidal cells onto aspiny interneurons of cat visual cortex. *J Physiol* 500: 689–713, 1997.
- Buzsáki G, Urioste R, Hetke J, and Wise K.** High frequency network oscillation in the hippocampus. *Science* 256: 1025–1027, 1992.
- Chance FS, Abbott LF, and Reyes AD.** Gain modulation from background synaptic input. *Neuron* 35: 773–782, 2002.
- Compte A, Sanchez-Vives MV, McCormick DA, and Wang X.-J.** Cellular and network mechanisms of slow oscillatory activity (<1 Hz) and wave propagations in a cortical network model. *J Neurophysiol* 89: 2707–2725, 2003.
- Connor JA, Walter D, and McKown R.** Neural repetitive firing—modifications of the Hodgkin–Huxley axon suggested by experimental results from crustacean axons. *Biophys J* 18: 81–102, 1977.
- Connors BW, Gutnick MJ, and Prince DA.** Electrophysiological properties of neocortical neurons in vitro. *J Neurophysiol* 48: 1302–1320, 1982.
- Csicsvari J, Hirase H, Czurko A, and Buzsáki G.** Reliability and state dependence of pyramidal cell–interneuron synapses in the hippocampus: an ensemble approach in the behaving rat. *Neuron* 21: 179–189, 1998.
- Csicsvari J, Hirase H, Czurko A, Mamiya A, and Buzsáki G.** Fast network oscillations in the hippocampal CA1 region of the behaving rat. *J Neurosci* 19: RC20, 1999a.

- Csicsvari J, Hirase H, Czurko A, Mamiya A, and Buzsáki G. Oscillatory coupling of hippocampal pyramidal cells and interneurons in the behaving rat. *J Neurosci* 19: 274–287, 1999b.
- Destexhe A, Contreras D, and Steriade M. Spatiotemporal analysis of local field potentials and unit discharges in cat cerebral cortex during natural wake and sleep states. *J Neurosci* 19: 4595–4608, 1999.
- Destexhe A and Paré D. Impact of network activity on the integrative properties of neocortical pyramidal neurons in vivo. *J Neurophysiol* 81: 1531–1547, 1999.
- Engel AK, König P, Kreiter AK, Schillen TB, and Singer W. Temporal coding in the visual cortex: new vistas on integration in the nervous system. *Trends Neurosci* 15: 218–226, 1992.
- Erisir A, Lau D, Rudy B, and Leonard CS. Function of specific K⁺ channels in sustained high-frequency firing of fast-spiking cortical interneurons. *J Neurophysiol* 82: 2476–2489, 1999.
- Ermentrout GB and Rinzel J. Beyond a pacemaker's entrainment limit: phase walk-through. *Am J Physiol* 246: 102–106, 1984.
- Fisahn A, Pike FG, Buhl EH, and Paulsen O. Cholinergic induction of network oscillations at 40 Hz in the hippocampus in vitro. *Nature* 394: 186–189, 1998.
- Fourcaud-Trocmé N, Hansel D, van Vreeswijk C, and Brunel N. How spike generation mechanisms determine the neuronal response to fluctuating inputs. *J Neurosci* 23: 11628–11640, 2003.
- Fries P, Neunschwander S, Engel AK, Goebel R, and Singer W. Rapid feature selective neuronal synchronization through correlated latency shifting. *Nat Neurosci* 4: 194–200, 2001a.
- Fries P, Reynolds JH, Rorie AE, and Desimone R. Modulation of oscillatory neuronal synchronization by selective visual attention. *Science* 291: 1560–1563, 2001b.
- Fuhrmann G, Markram H, and Tsodyks M. Spike frequency adaptation and neocortical rhythms. *J Neurophysiol* 88: 761–770, 2002.
- Gabbiani F and Koch C. Principles of spike train analysis. In: *Methods in Neuronal Modeling*, edited by Koch C and Segev I. Cambridge, MA: MIT Press, 1998, p. 313–360.
- Gerstner W. Population dynamics of spiking neurons: fast transients, asynchronous states, and locking. *Neural Comput* 12: 43–89, 2000.
- Gerstner W, van Hemmen L, and Cowan J. What matters in neuronal locking? *Neural Comput* 8: 1653–1676, 1996.
- Gupta A, Wang Y, and Markram H. Organizing principles for a diversity of GABAergic interneurons and synapses in the neocortex. *Science* 287: 273–278, 2000.
- Hansel D, Mato G, and Meunier C. Synchrony in excitatory neural networks. *Neural Comput* 7: 307–337, 1995.
- Häusser M, Major G, and Stuart GJ. Differential shunting of EPSPs by action potentials. *Science* 291: 138–141, 2001.
- Hodgkin AL and Huxley AF. A quantitative description of membrane current and its application to conductance and excitation in nerve. *J Physiol* 117: 500–544, 1952.
- Klausberger T, Magill PJ, Marton LF, Roberts JDB, Cobden PM, Buzsáki G, and Somogyi P. Brain-state- and cell-type-specific firing of hippocampal interneurons in vivo. *Nature* 421: 844–848, 2003.
- Knight BW. Dynamics of encoding in a population of neurons. *J Gen Physiol* 59: 734–766, 1972.
- Kopell N and LeMasson G. Rhythmogenesis, amplitude modulation, and multiplexing in a cortical architecture. *Proc Natl Acad Sci USA* 91: 10586–10590, 1994.
- Kraushaar U and Jonas P. Efficacy and stability of quantal GABA release at a hippocampal interneuron–principal neuron synapse. *J Neurosci* 20: 5594–5607, 2000.
- Lacaille J and Williams S. Membrane properties of interneurons in stratum oriens-alveus of the CA1 region of rat hippocampus in vitro. *Neuroscience* 36: 349–359, 1990.
- Lien C-C, Martina M, Schultz JH, Ehmke H, and Jonas P. Gating, modulation and subunit composition of voltage-gated K⁺ channels in dendritic inhibitory interneurons of rat hippocampus. *J Physiol* 538: 405–419, 2002.
- Logothetis NK, Pauls J, Augath MA, Trinath T, and Oeltermann A. Neurophysiological investigation of the basis of the fMRI signal. *Nature* 412: 150–157, 2001.
- Marder E. From biophysics to models of network function. *Annu Rev Neurosci* 21: 25–45, 1998.
- Markram H, Lubke J, Frotscher M, Roth A, and Sakmann B. Physiology and anatomy of synaptic connections between thick tufted pyramidal neurons in the developing rat neocortex. *J Physiol* 500: 409–440, 1997.
- Martina M and Jonas P. Functional differences in Na⁺ channel gating between fast-spiking interneurons and principal neurons of rat hippocampus. *J Physiol* 505: 593–603, 1997.
- Martina M, Schultz JH, Ehmke H, Monyer H, and Jonas P. Functional and molecular differences between voltage-gated K⁺ channels of fast-spiking interneurons and pyramidal neurons of rat hippocampus. *J Neurosci* 15: 8111–8125, 1998.
- Nomura M, Fukai T, and Aoyagi T. Synchrony of fast-spiking interneurons interconnected by GABAergic and electrical synapses. *Neural Comput* 15: 2179–2198, 2003.
- Nowak LG, Azouz R, Sanchez-Vives MV, Gray CM, and McCormick DA. Electrophysiological classes of cat primary visual cortical neurons in vivo as revealed by quantitative analyses. *J Neurophysiol* 89: 1541–1566, 2003.
- Pesaran B, Pezaris JS, Sahani M, Mitra PP, and Andersen RA. Temporal structure in neuronal activity during working memory in macaque parietal cortex. *Nat Neurosci* 5: 805–811, 2002.
- Press WH, Teukolsky SA, Vetterling WT, and Flannery BP. *Numerical Recipes in C*. Cambridge, UK: Cambridge Univ. Press, 1992.
- Richardson MJ, Brunel N, and Hakim V. From subthreshold to firing rate resonance. *J Neurophysiol* 89: 2538–2554, 2003.
- Shriki O, Hansel D, and Sompolinsky H. Rate models for conductance-based cortical neuronal networks. *Neural Comput* 15: 1809–1841, 2003.
- Shu Y, Hasenstaub A, and McCormick DA. Turning on and off recurrent balanced cortical activity. *Nature* 423: 288–293, 2003.
- Softky W. Sub-millisecond coincidence detection in active dendritic trees. *Neuroscience* 58: 13–41, 1994.
- Tamas G, Buhl EH, and Somogyi P. Fast IPSPs elicited via multiple synaptic release sites by different types of GABAergic neurons in the cat visual cortex. *J Physiol* 500: 715–738, 1997.
- Tamas G, Somogyi P, and Buhl EH. Differentially interconnected networks of GABAergic interneurons in the visual cortex of the cat. *J Neurosci* 18: 4255–4270, 1998.
- Traub RD, Whittington MA, Collins SB, Buzsáki G, and Jefferys JGR. Analysis of gamma rhythms in the rat hippocampus in vitro and in vivo. *J Physiol* 493: 471–484, 1996.
- van Vreeswijk C, Abbott L, and Ermentrout GB. When inhibition not excitation synchronizes neural firing. *J Comput Neurosci* 1: 313–321, 1994.
- Vida I, Halasy K, Szinyei C, Somogyi P, and Buhl EH. Unitary IPSPs evoked by interneurons at the stratum radiatum–stratum lacunosum moleculare border in the CA1 area of the rat hippocampus in vitro. *J Physiol* 506: 755–773, 1998.
- Wang X-J. Calcium coding and adaptive temporal computation in cortical pyramidal neurons. *J Neurophysiol* 79: 1549–1566, 1998.
- Wang X-J and Buzsáki G. Gamma oscillation by synaptic inhibition in a hippocampal interneuronal network model. *J Neurosci* 16: 6402–6413, 1996.
- Xiang Z, Huguenard JR, and Prince DA. GABAA receptor mediated currents in interneurons and pyramidal cells of rat visual cortex. *J Physiol* 506: 715–730, 1998.
- Zhang K and McBain CJ. Potassium conductances underlying repolarization and after-hyperpolarization in rat CA1 hippocampal interneurons. *J Physiol* 488: 647–660, 1995.
- Zhou F-M and Hablitz JJ. AMPA receptor-mediated EPSCs in rat neocortical layer II/III interneurons have rapid kinetics. *Brain Res* 780: 166–169, 1998.